DNA BASED THIN FILM AS HOLE TRANSPORT LAYER IN BULK HETEROJUNCTION POLYMER SOLAR CELLS

by

VIDYALAKSHMI KOLACHURE

Presented to the Faculty of the Graduate School of

The University of Texas at Arlington in Partial Fulfillment

of the Requirements

for the Degree of

MASTER OF SCIENCE IN MATERIAL SCIENCE AND ENGINEERING

THE UNIVERSITY OF TEXAS AT ARLINGTON

August 2007

ACKNOWLEDGEMENTS

I would like to thank my supervising professor Dr Michael Jin for his guidance, encouragement and advice throughout the research. Also, I would like to thank my dissertation committee members Dr Pranesh Aswath and Dr Choongun Kim.

I thank Characterization Center for Materials and Biology (C^2MB) for allowing me to use the characterization tools and also thank all the material science faculty and staff.

I would like to thank Xin for helping me carry out Cyclic Voltammetry measurements and depositing the top electrode. I also thank Karan and Chun Young for their help while using different instruments.

Lastly, I would like to thank my husband, Prasanna for his support and encouragement throughout the study. Also, I thank my parents for their love and support in everything I have accomplished.

July 26, 2007

ABSTRACT

DNA BASED THIN FILM AS HOLE TRANSPORT LAYER

IN BULK HETEROJUNCTION POLYMER

SOLAR CELLS

Publication No. _____

Vidyalakshmi Kolachure, M.S

The University of Texas at Arlington, 2007

Supervising Professor: Dr Michael Jin

In the field of organic solar cell, the conjugated polymer-fullerene bulk heterojunction concept is one of the ongoing research interests. In this work, the use of de-oxyribose nucleic acid/ hexadecyl trimethyl ammonium chloride (DNA/CTMA) thin films as hole transport layer in poly(3-hexylthiophene)-methanofullerene (P3HT-PCBM) bulk heterojunction polymer solar cell is demonstrated. P3HT-PCBM bulk heterojunction polymer solar cell was fabricated with a DNA complex layer replacing commonly used PEDOT-PSS (poly(3,4-ethylenedioxythiophene)-poly(styrenesulfonate) (PEDOT-PSS). While PEDOT-PSS, as a hole transport and electron blocking layer, often improves the solar cell performance by improving fill factor, it requires careful

engineering of spin-coating for the aqueous solution of PEDOT-PSS because of the hydrophobic nature of indium tin oxide on which PEDOT-PSS is generally deposited. Contrarily butanol solution of the DNA complex easily wets any oxide surface effectively forming DNA complex thin film. Subsequent spin-coating of P3HT-PCBM solution does not dissolve the DNA layer either. The band-gap of DNA complex layer is about 4.1 eV and it is transparent to broad spectrum of UV and visible light. The DNA complex layer is well known hole transport layer and its lowest unoccupied molecular orbital is quite high (1.1 eV) blocking electron quite efficiently.

In this work, we report the use of DNA complex layer in polymer solar cell structure for the first time and provide the indirect evidence of hole conduction in DNA complex layer. Optical absorption for individual layers was carried out and the band gap of DNA complex layer was extracted from the transmittance data. Cyclic voltammetry for DNA complex layer was carried out for the first time and the signal of oxidation was observed which relates to the oxidation of the guanine bases. From this oxidation peak, highest occupied molecular orbital (HOMO) level of DNA complex layer was found and used for the band alignment of the solar cell.

TABLE OF CONTENTS

LIST OF ILLUSTRATIONS

LIST OF TABLES

CHAPTER 1

INTRODUCTION

The polymer based solar cell is a promising field in organic solar cell research due to ease of processing and increasing efficiencies. The biomaterial DNA (De-oxyribose nucleic acid) is used in this study in the making of bulk heterojunction polymer solar cell.

The improvement in properties such as solubility in organic solvents, transparency and feasible band gap attained when DNA complex is formed motivated us to incorporate DNA complex in solar cell devices as a hole transport layer. The advantages of replacing the commonly used poly(3,4-ethylenedioxythiophen) /polystyrene sulfonic acid (PEDOT-PSS) by DNA complex layer as a hole transport layer are: (a) it also serves as an electron blocking layer by preventing electrons from reaching the indium tin oxide (ITO), due to its high lowest unoccupied molecular orbital (LUMO) level, (b) wets ITO very well as it is soluble in organic solvents whereas PEDOT-PSS (Poly(3,4-ethylenedioxythiophene)-polystyrenesulfonate) is a water dispersion, and (c) DNA provides better transparency than PEDOT-PSS potentially increasing photocurrent. Moreover, DNA complex layer can be used to study the transport of hole only devices by placing it in front of cathode preventing electron current.

The following sections of the thesis briefly explain the operational principle of various types of solar cells including organic solar cells, their device architecture, and recent developments in DNA electronics.

1.1 Solar Cells

The process of conversion of light into electricity is called as Photovoltaic effect. This was first observed by Becquerel in 1839 [1]. The field of study related to solar cells is known as photovoltaics. Solar cells have been used in remote applications where electric power cannot be reached. It has been used to power up satellites, and consumer electronics like watches, calculators and in remote water pumping applications.

The first generation photovoltaics represented by crystalline silicon solar cells are also called as bulk-based solar cells. It typically consists of a large area, p-n homojunction diodes on thick wafer and converts light energy to electrical energy. They are the dominant technology which encompasses 86% of the production of the solar cell market as of 2007.

The second generation photovoltaics are based on thin-films of semiconductor materials deposited on different types of substrates such as glass, metal foil, and polymers. These take the advantage of using a thin film of material in turn reducing the mass of the material required for the cell design, thereby reducing the cost of the material. Some of the materials used in this generation are amorphous silicon, chalcopyrite compounds represented most often by copper indium gallium selenide (CIGS), and cadmium telluride [2].

The third generation photovoltaic materials include the excitonic organic solar cells, photoelectrochemical cells, and quantum dot solar cells. These are different from the traditional solar cells as they do not depend on the typical layered p-n junction to separate the photogenerated charge carriers, but depend on the dissociation of the excitons to form free charge carriers and these free carriers have to travel through the polymer to the respective electrodes.

1.2 Solar Irradiation and tandem solar cells

The sun's radiation intensity has a spectrum that resembles the radiation of black body at a temperature of about 6000 K [3]. The spectrum of solar energy is shown in Figure 1. The solar irradiation outside atmosphere and at the sea level corresponds to AM0 and AM1.5 respectively. Air-mass zero or solar constant is the amount of solar radiation per unit area measured on outer surface of the earth's atmosphere perpendicular to the direction of the sun. This is a constant and has a value of 1366 W/m^2 [4]. The intensity of radiation reaching the earth depends on the absorption and scattering effects of the atmosphere. The solar spectrum in the figure shows some sharp peaks at some wavelengths due to the absorption from water vapor molecules, ozone and by air. The atmosphere controls the amount of solar radiation reaching the earth's surface and also the amount of radiation escaping from the surface of the earth.

Air mass one is attained when the sun is directly above the location and sun rays takes the shortest path to the earth's surface and the spectrum is called AM1 [3]. Air mass is defined as the ratio of the actual radiation path to the shortest path.

The standard conditions used to test terrestrial solar cells are AM 1.5 and light intensity corresponds to 1000 W/m^2 and the temperature of the cell maintained at 25°C. Also, the output power is given in peak watts.

In order to utilize large spectrum of solar light, tandem solar cells are developed. The tandem solar cells are made by stacking these multi-spectrum layers on top of each other. By stacking one above the other, it forms tandem cell where in the first layer receives the high energy part of the spectrum, the second layer receives the visible part and the last layer receives the infrared spectrum of light thereby harvesting significant light energy.

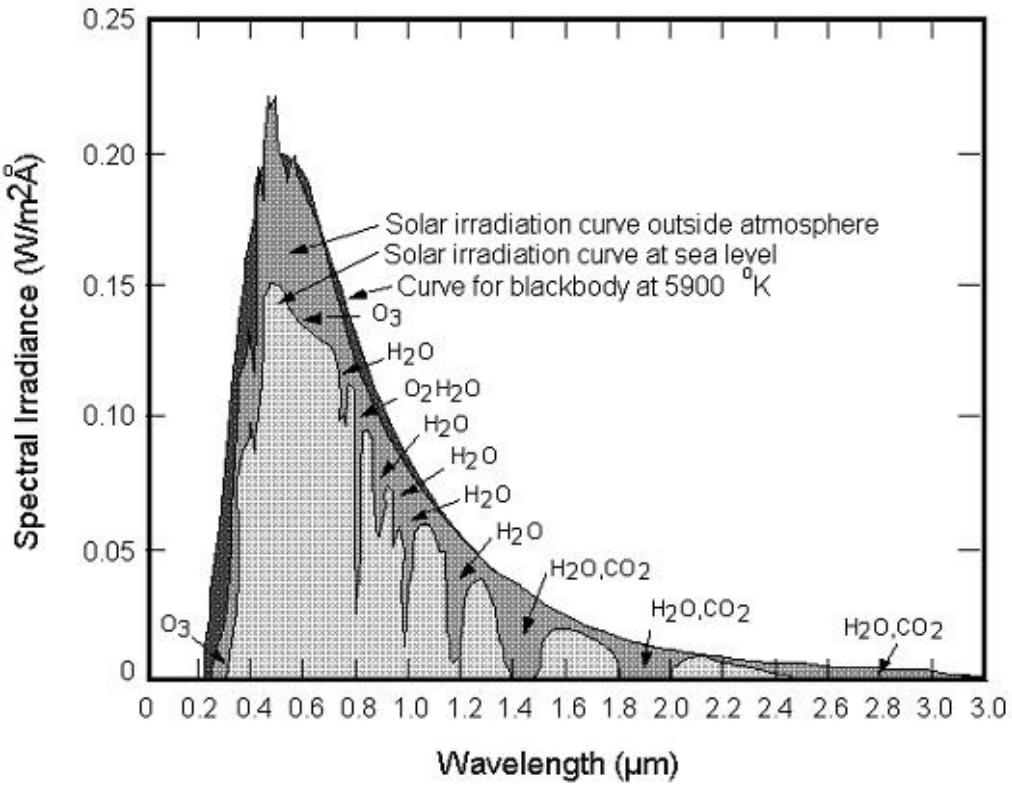

Figure1: Solar Spectrum [5]

1.3 Solar Cell Characteristics

A typical current versus voltage plot is as shown below in Figure 2. This is the plot of the terminal voltage of the cell under varying loading conditions. In this plot, load is varied from open circuit (no load) all the way to short circuit condition, and the corresponding terminal voltage is shown.

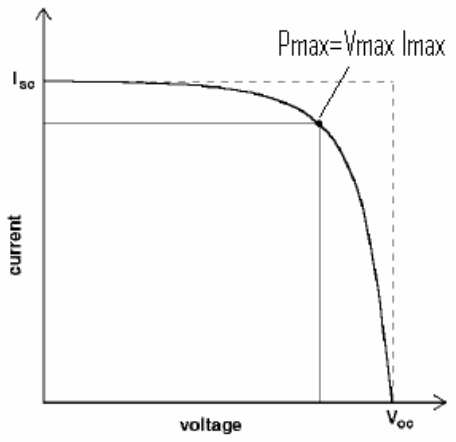

Figure 2: I-V curve of a typical solar cell. (Symbols corresponds to I_{sc}= Short circuit current, V_{oc}= Open circuit Voltage, P_{max} = Maximum Power point)

1.3.1 Open Circuit Voltage (V_{oc})

When a solar cell is exposed to light, a voltage is developed. The voltage developed when the two terminals of the cell are not connected is called the open circuit voltage. It is represented by V_{oc}. Under open circuit conditions, the current cannot flow and the voltage is at its maximum.

1.3.2 Short Circuit Current (I_{sc})

The current drawn when the two terminals of the cell are connected is called the short circuit current, and is represented by I_{sc}.

1.3.3 Maximum Power Point (P_{max})

The point in the I-V curve where the product of the voltage and the current is at its maximum is called the maximum power point. It is $P_{max} = V_{max}I_{max}$.

1.3.4 Fill Factor (FF)

Fill factor is the measure of the squareness of the I-V curve. It is defined as follows,

$$FF= V_{max} I_{max}/ V_{oc}I_{sc}$$

1.3.5 Quantum Efficiency

Quantum Efficiency is the probability that an incident photon will deliver one electron to the external circuit.

1.3.6 Power Conversion Efficiency (η)

Power conversion efficiency (PCE) is the ratio of the maximum power obtained to the power input.

$$\eta = P_{output} / P_{input}$$

$$= V_{max} I_{max}/ P_{input}$$

$$= V_{oc}I_{sc} FF/ P_{input}$$

1.4 Inorganic Silicon solar cells

The generic p-n junction consists of a thin heavily doped n-type layer (emitter) sandwiched with a thick moderately doped p-type layer (base). The bottom surface is covered with a metal and the topside with an anti-reflection coating and a metal grid which act as electrodes. The schematic is as shown in Figure 3.

The n–type layer and p-type layer is formed by doping Si with group V and group III elements of the periodic table respectively. When the n-type and p-type layer are in contact there is transport of electrons and holes across the interface until it reaches equilibrium and forms a depletion zone or space charge region. In this region there are no free charge carriers but a built-in-electric field is observed.

When light is illuminated on the cell, most of the photons are absorbed by the depletion region and the p-type layer and creates electron hole pairs as the n-type is very narrow. The free carriers generated in the depletion region and in the n and p type layers which are within their diffusion length are separated by the built-in-electric field. The electron drifts and reaches the n side and the hole drifts to the p side. This process generates open circuit voltage between the terminals of the device with the p side positive with regard to the n side. When a load is connected across the terminals of the device, current flows through the device.

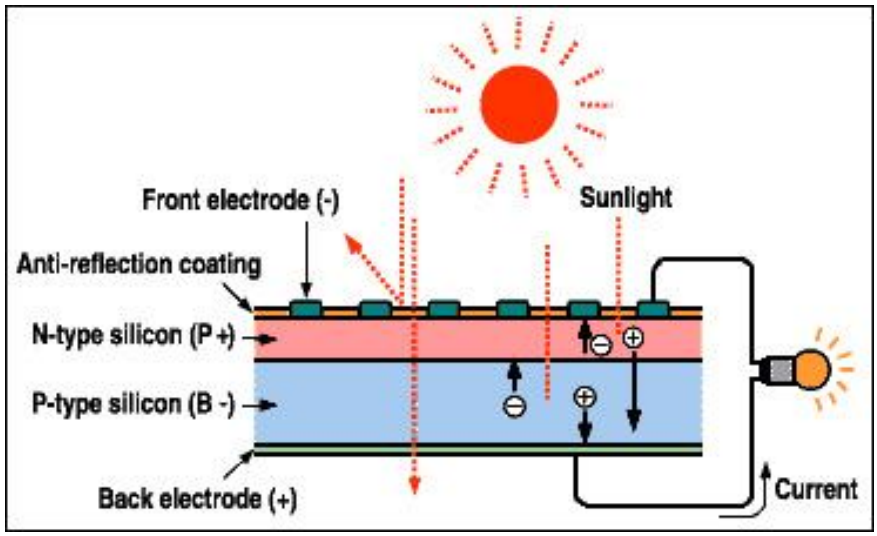

Figure 3: Cross section view of a typical silicon solar cell [6].

1.5 Organic Solar Cells

A solar cell which incorporates organic molecules is called organic solar cell. They offer several advantages like the organic molecules are inexpensive, and they have broad absorption band in the visible spectrum which increases the absorption coefficient and in turn provides the ability to scale down the thickness of the films to few hundred nanometers. Also, they can be manufactured at low temperatures using doctor blade method, spin coating or roll to roll printing. The latter can be done on a large scale manufacturing. Moreover, low temperature capability allows them to be fabricated on flexible plastic substrates, making them light weight.

Organic solar cells are also called as “excitonic” solar cells because the absorption of light by the solar cell creates excitons - bound electron hole pairs – instead of free carriers. Excitons are created upon light absorption because of low dielectric constants and weak inter-molecular bonding [7]. In case of organic and inorganic solar cells difference exists in the exciton binding energy. In case of inorganic semiconductors, the exciton binding energy is small and hence free charge carriers are created at room temperature. Whereas, in organic materials, the exciton binding energy exceeds the thermal energy at room temperature, and hence forms excitons. These excitons have to diffuse to the donor-acceptor interface and then the excitons splits to form free charge carriers. The free carriers formed have to diffuse to the corresponding electrodes and are then collected by the electrodes.

1.6 Dye sensitized solar cells

These cells have reached an efficiency of about 11% [8] reported by Grätzel et al. In this cell, small organic dye molecules are adsorbed onto the surface of the TiO_2 molecules and an electrolyte containing reduction-oxidation couple such as Iodide/tri-iodide (I^-/I_3^-) and a catalyst coated counter electrode is used. These dye molecules absorbs light and the electron is injected from the dye to the TiO_2 and passed to the electrolyte thereby reaching the electrode. The schematic of a dye sensitized solar cell is shown in Figure 4 below.

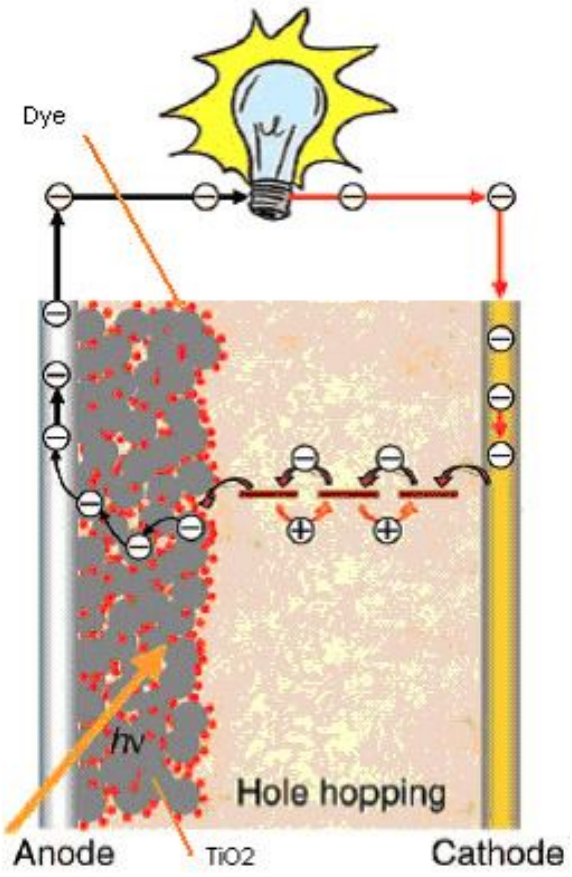

Figure 4: Working principle of dye sensitized solar cell [8]

1.7 Organic solar cell Architectures

There are several architectures of organic solar cell namely single layer, bilayer and bulk heterojunction structures. The newer development among these structures is to obtain better cell efficiencies by improving the charge separation and collection processes in the materials. The thickness of the organic layers is typically in the range of few hundred nanometers. The schematic of the different types of organic cell structure is shown in Figure 5. The top and bottom contacts used are ITO and Aluminum which represent the high work function and low work function electrodes respectively.

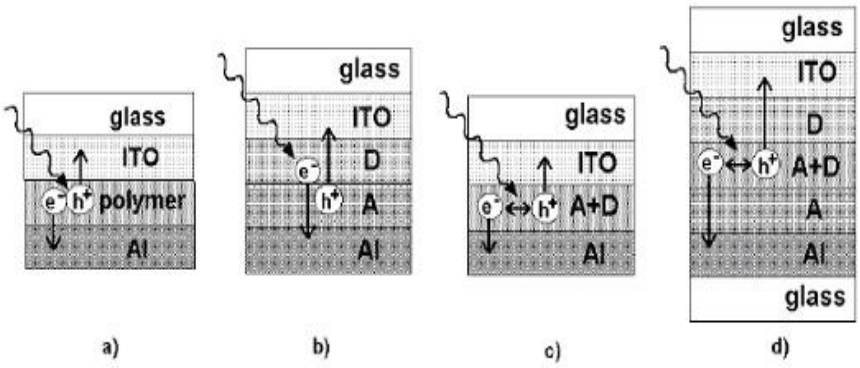

Figure 5: Organic photovoltaic device architectures a) Single layer, b) donor-acceptor bilayer, c) donor-acceptor bulk heterojunction and d) donor-acceptor laminated structure (D and A stand for electron-donating and electron-accepting layers respectively) [9]

1.7.1 Single layer devices

In case of single layer devices, a conjugated polymer is sandwiched between the two electrodes, ITO and Al which have different work functions [9]. The

dissimilar work functions of the electrodes sets up an electric field through the polymer when they are short circuited by connecting them to the external circuit. The movement of electrons from the low work-function electrode (Al) to the high work-function electrode (ITO) is the root cause for the generating of this electric field and is crucial to the operation of the cell.

Metal-Insulator-Metal (MIM) tunnel diode model shown in Figure 5a explains the behavior of such a device. The electric field generated between the electrodes dissociates the excitons and transports the charge carriers to the opposite electrodes, generating the current. The behavior of single layer device is highly influenced by the free carrier concentration, which in turn depends on the impurity density of the polymer. It should be noted that, although the MIM model explains the behavior of the cell at low impurity concentrations, at higher impurity concentrations, the Schottky diode model better explains the cell behavior.

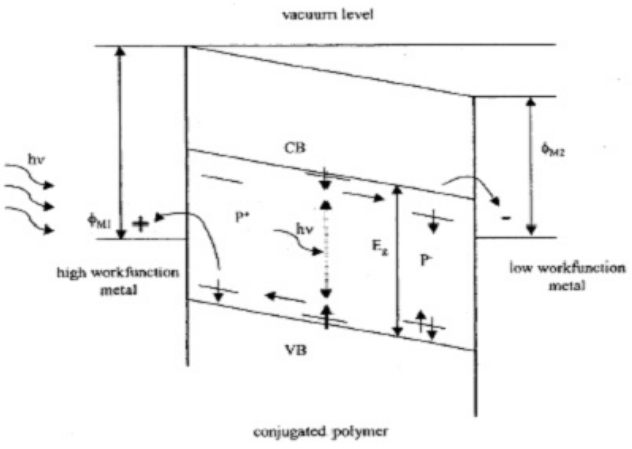

Figure 6: Band diagram for the MIM model of a single layer conjugated polymer photovoltaic device under short circuit conditions. (VB-valence band, CB-conduction band, E_g-band gap energy, excitons respectively) [10]

Although single layer polymer cells exhibit significant current rectifying properties in the photovoltaic cell mode, their energy conversion efficiency is rather low, typically around 0.1%. This is mainly due to the fact that the electrical field generated across the polymer is solely due to the work difference between the electrodes, and is very low. This potential difference and thus the associated electric field is not high enough for efficient exciton dissociation in the polymer [10].

Another shortcoming with the single layer devices is the fact that both the electrons and holes need to travel in the same material, and hence the recombination losses are quite high. In single layer devices with high impurity concentration (Schottky type devices) the photoactive region is usually very thin, and close to one of the electrodes. The bulk of the organic layer is inactive, and works as an optical filter if the cell is illuminated from the inactive side, further contributing to the low efficiency. One exception to the low efficiency single layer cells is the bromine doped pentacene crystal based single layer organic solar cell which have demonstrated PCE of greater than 4.5% [11] under standard AM1.5 illumination.

While the pentacene crystals are grown by horizontal physical vapor transport in a stream of hydrogen in 200-300°C temperature and the thin film deposition requires vapor deposition. Both vapor transport and vapor deposition being expensive process, have prevented these types of cells from being an economical solution to energy conversion needs. This may be considered as a serious drawback compared to the organic solar cells which are deposited at room temperature from solutions, a highly economical process.

1.7.2 Donor-acceptor bilayer devices

To overcome some of the short comings of the single layer cells, mainly their lower efficiency due to recombination, donor-acceptor bi-layer cells are developed (Figure 7). In these cells, the two layers, one containing electron accepting molecules (A) and one containing electron donating layers (D) are used. Majority of the light is absorbed by the electron donating layer and creates excitons. Excitons have to dissociate to form free charge carriers and this process takes place at the D-A layer interface, and due to the relative high energy difference between these layers the dissociation process is greatly enhanced. Having two individual layers separates the electron and hole transportation, greatly reducing the recombination. Moreover, since active region in which splitting process takes place extends into both the D and the A layers, it is almost double compared to single layer cells. Moreover, using two different semiconductors allows the band gaps to be tuned to match better the solar spectrum [12].

Conjugated polymers [13], organic macromolecules [14], pigments [15] or dyes [16] can all be utilized as donor and acceptor molecules. Out of the published research work, Tang [15] reached about 1% PCE with a bilayer organic solar cell consisting of vacuum evaporated copper phthalocyanine (CuPc) and perylene derivative (PV) pigment layers, standing as one of the best results among organic solar cells. But recent efforts to fabricate Tang's cell with soluble derivatives (dyes) of CuPc and perylene by Petritsch et al. [16] considerably lowered the cell performance. Another example of an efficient bilayer organic solar cell is the ZnPc | PTCDIa (Perylene tetracarboxylic Acid

Diimides) bilayer device with a 0.43% PCE [17], and an example of a polymer | polymer bilayer device is the cell by Jenekhe & Yi [13] with a 0.7% PCE. The most efficient organic bilayer solar cell within author's knowledge, however, is a vacuum evaporated pigment based CuPc | C_{60} device by Peumans [18] with a 3.6% PCE at 150 mW/cm^2 AM1.5 illumination.

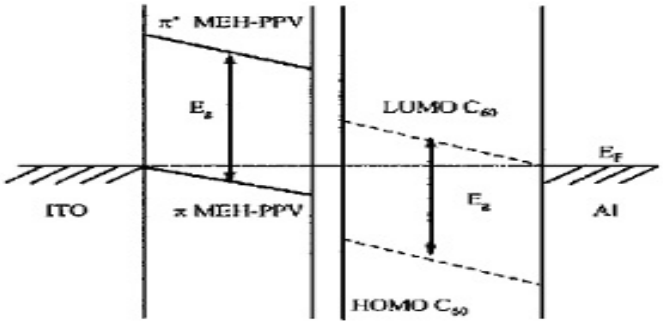

Figure 7: Band diagram of a bilayer donor-acceptor device under short circuit conditions. MEH-PPV is the electron-donating polymer, and C_{60} is the electron acceptor [10].

1.7.3 Donor-acceptor bulk-heterojunction or blend devices

The planar donor-acceptor junction increase the cell efficiency by doubling the active region of the solar cell compared to the single layer device. Although this improves the efficiency quite a bit, it has not been enough where high efficiency cells are required because of the short exciton diffusion length of about <20nm [7]. To further increase the optical thickness of the cell while maintaining efficient current collection, the concept of interpenetrating network of electron-accepting and electron-donating molecular species has been developed [19-21] and demonstrated successfully in number of different so-called donor-acceptor bulk-heterojunction or blend devices.

These cells employ a phase separated blend of organic donor and acceptor semiconductor materials with domains not larger than twice the exciton diffusion length. This increases the thickness of the active exciton dissociation region. This type of cell mandates an interpenetrating structure of the donor and acceptor phases instead of a random blend. This is because every site within the donor and acceptor phases should be contacted to the opposite electrodes by the respective materials. Any isolated domain of either donor or acceptor material would be optically active but electrically inactive, reducing the efficiency of the photovoltaic cell.

Donor-Acceptor laminated polymer device designed by [22] serves as an intermediate device of the bilayer and the bulk heterojunction structure. The device comprised of individually prepared films of cyano derivative of poly(p-phenylene vinylene) and derivative of polythiophene i.e, poly-[2-methoxy-5-(2'-ethylhexyloxy)-1,4-(1-cyanovinylene)-phenylene]: poly(3- (4-octylphenyl) thiophene), (MEH-CN-PPV:POPT) (19:1) blend on glass substrate coated with aluminum or calcium and a MEH-CN-PPV:POPT (19:1) blend on glass substrate coated with ITO or polyethylenedioxy thiophene, PEDOT, which were pressed at high temperatures to form a laminate. This resulted in an interpenetrating layer of the donor and the acceptor materials around 20-30nm thick. This resulted in a concentration gradient in the active layer from the donor and the acceptor material which is considered to be a plus point for the cell operation and a PCE of about 2% was achieved under 77 mW/cm^2 AM1.5 illumination.

The devices made with bulk heterojunction structure using fullerenes and semiconducting polymers as the active layer has shown the best efficiencies among polymer based organic solar cells; PCE of 2.5% was reported [23] using poly[2-methoxy-5-(3,7-dimethyloctyloxy)-1,4-phenylenevinylene] (MDMO-PPV) and methanofullerene (PCBM) as the donor and the acceptor material respectively. PCE of 4% is reported [24] wherein poly(3-hexylthiophene), (P3HT) and PCBM is used as an active layer where they report a correlation between preparing the device and its performance. High efficiency of 4.4% is reported by using P3HT and PCBM [25]. Heeger's group has reported the highest PCE of 6.5% by utilizing bulk heterojunction structure in tandem solar cells more recently [26].

As discussed earlier, the operation of an organic solar cell, involves the following processes. Initially the light has to be absorbed by the material to form excitons. Secondly the excitons have to diffuse to a region where the charges can be separated. Finally the charge has to be transported to the respective electrode i.e., holes to the anode and electrons to the cathode which contribute towards electric current.

Figure 8 shows that the donor material (P3HT) and the acceptor material (PCBM) are blended together to form a bulk heterojunction and DNA-CTMA is used as a hole transport layer. When light is illuminated on the cell, the polythiophene absorbs the light and creates excitons. These excitons diffuse to the interface and dissociate to form free electrons and holes. Then, the electrons go through PCBM and reach the top metal electrode whereas the holes travel through P3HT and reach the bottom electrode. The advantage of intermixing donor and the acceptor is to create a large interfacial area

which is less than the exciton diffusion length so that a large number of excitons can reach the interface and dissociate forming free charge carriers.

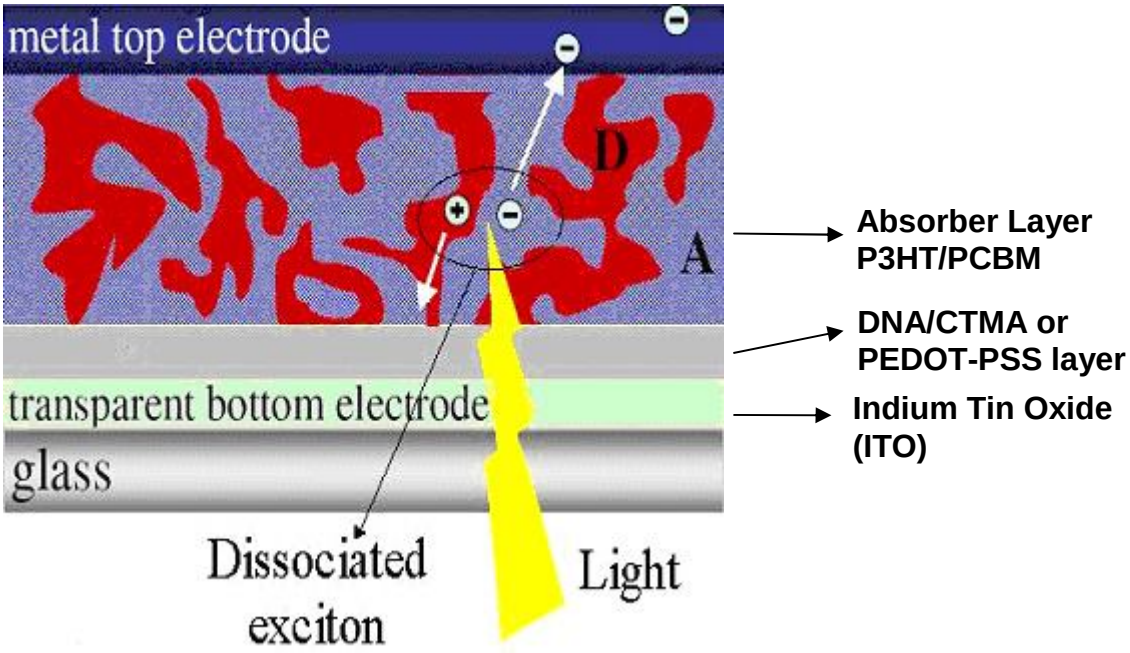

Figure 8: Cross sectional view of a bulk heterojunction solar cell. [7]

CHAPTER 2

INTRODUCTION TO DNA

This section of the thesis explains the basic properties of the de-oxyribose nucleic acid (DNA) as well as its charge transfer and conduction mechanism. The recently reported application of the DNA in a light-emitting diode (LED) is also described.

2.1 De-oxyribose nucleic acid (DNA)

DNA is the basic building block and the carrier of genetic information in all living organisms. It is a polymer made up of repeating monomeric units called nucleotide. Each nucleotide is made up of a 2-deoxyribose sugar, phosphate and a nitrogenous base about 0.34nm long [27]. Several nucleotides are linked together to form a polynucleotide chain which is single strand DNA. The bases are grouped into two types namely Purines and the Pyrimidines. Adenine and Guanine are Purines whereas Cytosine and Thymine are Pyrimidines. The structures of the bases are shown in Figure 9. Figure 10(a) shows the structure of a nucleotide and Figure 10(b) shows the complementary hydrogen bonding between the base pairs.

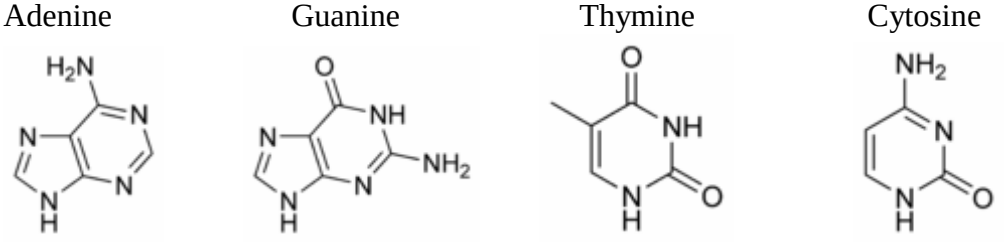

Figure 9: Structure of DNA bases [25]

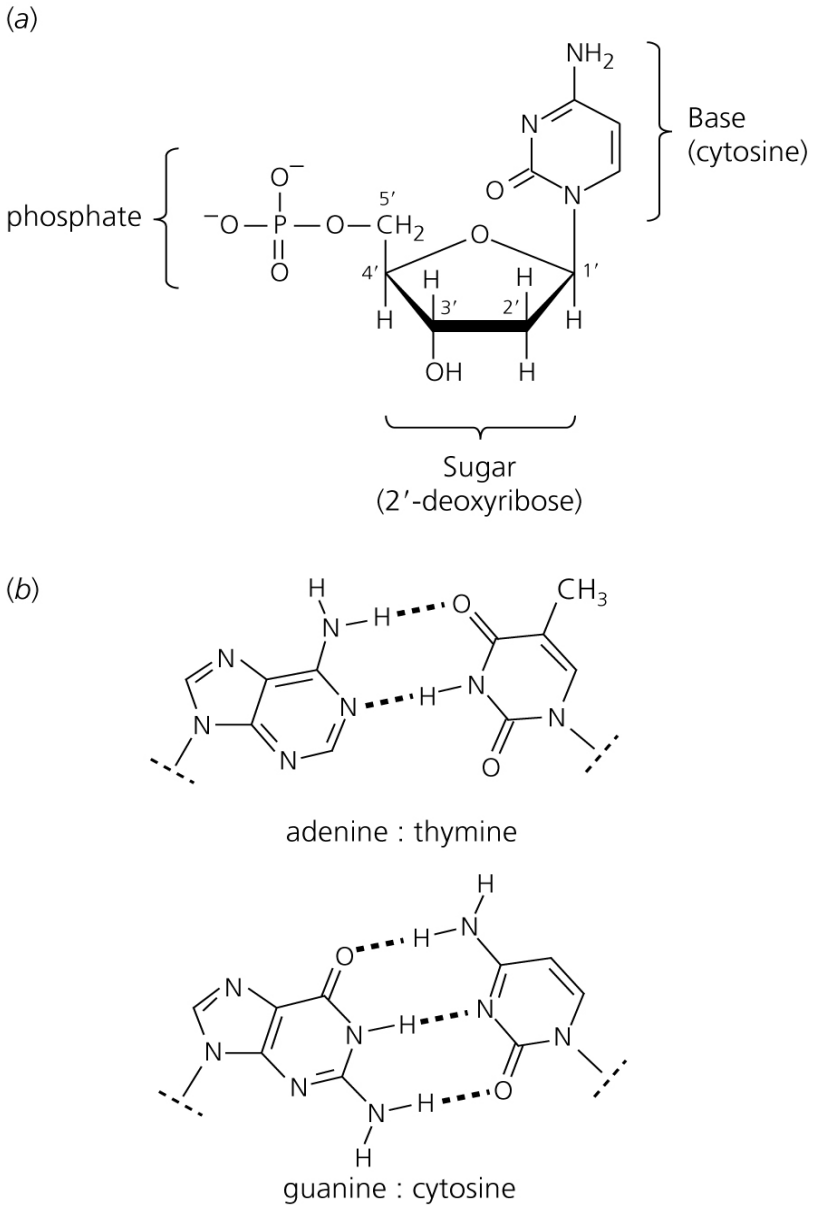

Figure 10: Structure of (a) Nucleotide, and (b) Complementary hydrogen bonding between the base pairs [28]

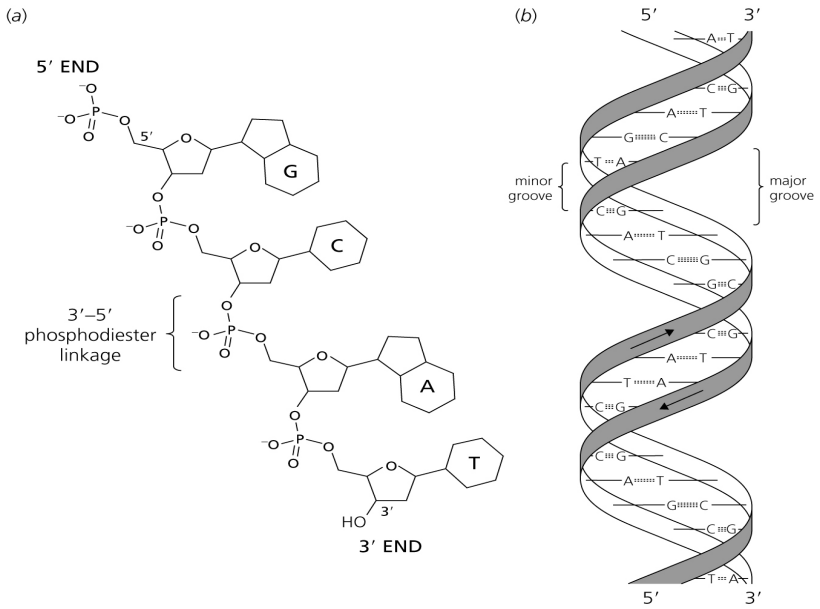

Figure 11: Structure of DNA [29]

In 1953, James D. Watson and Francis Crick were the first to discover the double helical structure of DNA. Figure 11(a) shows the structure of a polynucleotide chain and figure 11(b) shows the double helical structure of DNA. The alternating sugar and the phosphate ions make up the backbone of DNA providing mechanical stability to the double helix and protect the base pairs. The bases of the each nucleotide are on the inside of the helix which is stacked on top of each other. The phosphodiester bond is formed between two sugars and a phosphate group [28]. The two complementary single stranded DNA intertwine to form a double helix DNA which involves specific binding of Adenine (A) with Thymine (T) and Guanine (G) with Cytosine (C) through hydrogen bonds. This is called as hybridization. A forms two hydrogen bonds with T and G forms three hydrogen bonds with C as shown in figure. In a double strand DNA, the direction of each strand is opposite to that of the other strand and is called antiparallel. The

asymmetric ends of a strand are referred as the five prime (5') and the three prime (3') ends of DNA bases. The double helix forms two grooves that are of different widths and the larger groove is called the major groove and the smaller one is the minor groove. These grooves act as binding sites.

2.2 Charge Transfer in DNA

The charge transfer in DNA is of high interest due to its use in molecular electronics and biological concerns. Since DNA can be synthesized in any desired base sequence, and also the specific binding between the single strand DNA molecules have offered an opening to use DNA in self assembled molecular circuits for the application in nanoelectronics. The experiments carried out in solution chemistry have shown charge transfer in short DNA molecules and this has triggered interest among the scientific community to carry out further research to realize its use in complex electronic structures [30].

Daniel Eley and D.I Spivey were the first to put forward that DNA could serve as an electronic conductor as the electron orbitals of the bases overlap with each other along the z axis of the DNA [31]. However, experiments are reported wherein the conductivity induced by radiation is the result of the water molecules surrounding the double helix which are mobile charge carriers rather than occurring through the base-pair stack [32]. The reports on conduction properties in DNA are not consistent and it ranges from a conductor to an insulator.

DNA has been of interest in molecular electronics because of its two well known properties namely recognition of the molecule and self-assembly [33].

Molecular Recognition refers to the formation of a bond selectively with other molecules or with substrates. This property is based on the data stored in the structural features of the two interacting molecules. Self-assembly is the specific binding between the single strand DNA.

2.2.1 Superexchange Process and Molecular Wire

The charge transfer is said to occur by superexchange process or molecular wire. The factor that governs whether charge transfer occurs through superexchange or molecular wire mechanism is the energy level of the DNA (considered as the bridge) relative to the energy level of the donor and the acceptor [33]. Here, the donor and the acceptor molecules can be dyes or other molecules intercalated or covalently bonded to DNA molecule. The two processes are shown in Figure 12.

In case of superexchange process, the state of the DNA bridge lies above the level of the donor and the acceptor. When the donor is photoexcited, the electron is transferred to acceptor in one jump and is never localized in the DNA bridge. The rate of this process reduces exponentially with distance [33].

In case of a molecular wire, the state of the DNA bridge are quite comparable to that of the donor energy level. In this case, the electron can enter the DNA bridge. After injection, the electron is transferred to DNA bridge and then moves to the acceptor.

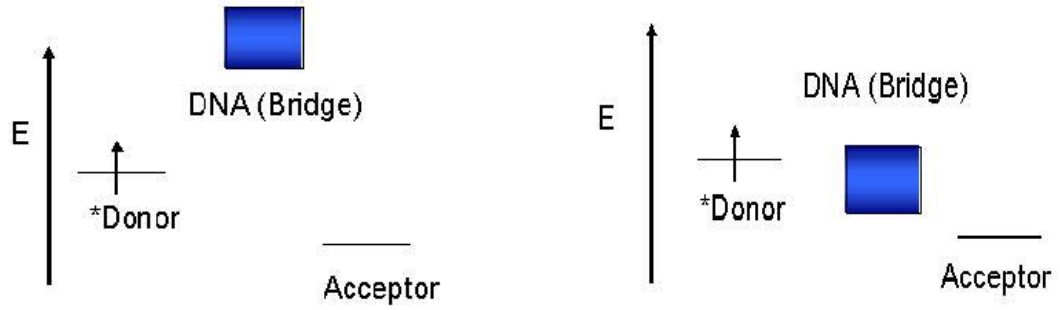

(a) (b)

Figure 12: Charge transfer in DNA (a) Superexchange process and (b) Molecular wire

2.3 Conduction Type of DNA

It is reported that the conductivity of DNA depends on several factors [31] like the base sequence on DNA, it's length, its form whether it is a single strand or double strand DNA, the environment i.e., the presence of water molecules or counter ions, the preparation conditions like if it is stretched or combed, whether it is attached to a surface or it is a free standing molecule and also on the detection protocols.

There have been several experiments carried out on charge conduction through DNA and it has been reported as an insulator to a semiconductor. The quantity normally used to distinguish this property is the bulk resistivity [30]. Another distinction used for DNA in regard to the experimental reproducibility is as follows. When a voltage is applied across a wide-bandgap polymer and if its structure is altered or damaged then it is an insulator, because the base-pair stacking is altered and affects the charge transport. And if its structure and properties is unaffected and there is charge transport induced in it, then it is considered as a wide-bandgap semiconductor.

Jacqueline Barton and his coworkers showed that DNA acts as conducting molecular wire [31]. In their work the donor and acceptor molecules were attached at known distances on the DNA through intercalation or covalent attachment (Figure 13), and they studied the photo-induced electron transfer between them. They measured the fluorescence on the excited molecule and found that it did not emit light when attached to a DNA molecule. They observed "fluorescence quenching" which was due to the charge on the excited donor molecule leaking along the length of the DNA to the acceptor molecule. Also this electron transfer was observed for a distance >40Å between donor and the acceptor molecules.

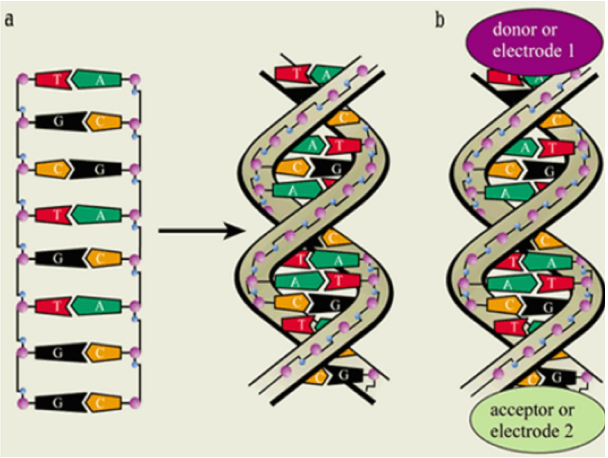

Figure 13: Schematic representation of (a) DNA double helix, (b) Donor and acceptor molecule attached to DNA [34]

It was reported by Braun and coworkers [35] that DNA acts as an insulator at room temperature. In their work they used λ-DNA, in which one end of the DNA was attached to gold electrodes chemically through sulfur - gold interactions. Up to ±10 V, they did not see any current.

The work done by Porath etal [36] shows that DNA acts as semiconductor. They carried out measurements by using short single stranded DNA with a tailored sequence of G-C base pairs which was freely hanged between two electrodes. The results indicated that no current was observed at low voltage and above 1V current was seen.

2.4 DNA based Organic Light Emitting Diode (OLED)

There have been a few studies which reported the use of DNA based thin film as an integral component in organic light emitting diodes. DNA complex layer was used in OLEDs [37] as a hole transport layer and electron blocking layer preventing electron–hole recombination occurring in the adjacent hole transport layers. Koyama *etal* [37] reported that DNA complex layer possesses both hole and electron transport abilities and preferentially transports holes due to a shallow lowest unoccupied molecular orbital (LUMO) level that prohibits an efficient electron injection from an adjacent carrier transport layer. In OLED characteristics (Figure 14) more recently reported by Hagen *et al*. It was concluded that the presence of DNA complex layer increased the brightness 30 times and it was ten times more efficient compared to the OLEDs without the use of DNA complex layer [38].

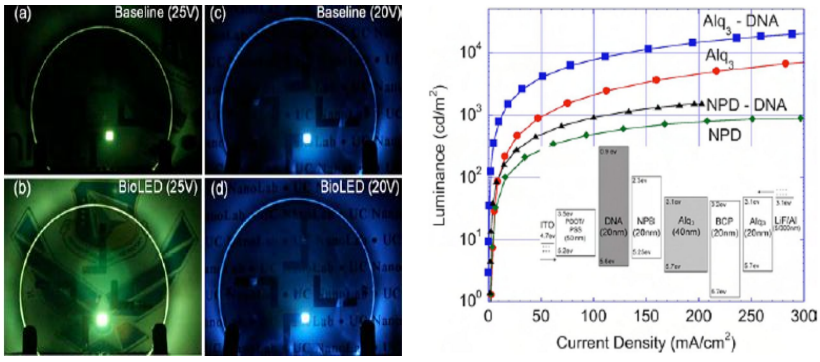

Figure 14: Organic LED with its characteristics [38].

CHAPTER 3

EXPERIMENTAL RESULTS

This section initially explains the structure of the device followed by a brief introduction to the various materials used in this study. The fabrication of each layer and its integration to form a bulk heterojunction solar cell is discussed. Further, experimental procedure of the cyclic voltammetry carried out on DNA based thin films together with the characterization techniques used in this study are summarized.

3.1 Device Architecture

The structure of the device fabricated in this study is shown in Figure 15. It consists of ITO coated glass used as the substrate and ITO acts as the bottom electrode over which the hole transport layer i.e., DNA complex or PEDOT-PSS layer is formed. Over this we have the active layer which is a blend of P3HT and PCBM where light is absorbed. Finally the top electrode Aluminum is deposited.

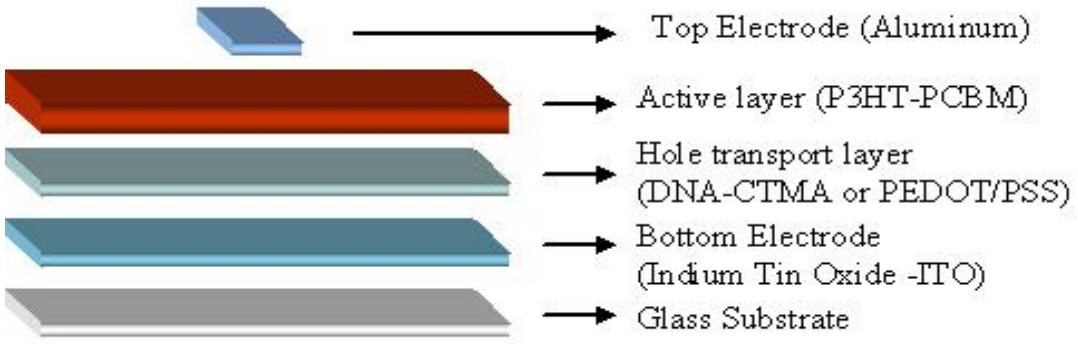

Figure 15: Structure of the solar cell fabricated in this study

3.2 PEDOT-PSS

Amongst the different conducting polymers, PEDOT-PSS has been the most widely used hole transport layer in numerous applications. It possesses several advantages like moderate band gap and good stability in the oxidized state. It shows high conductivity in the range of 400-600 S/cm [39], and is found to be highly transparent when thin films are made. The structure of PEDOT-PSS is as shown below (Figure 16).

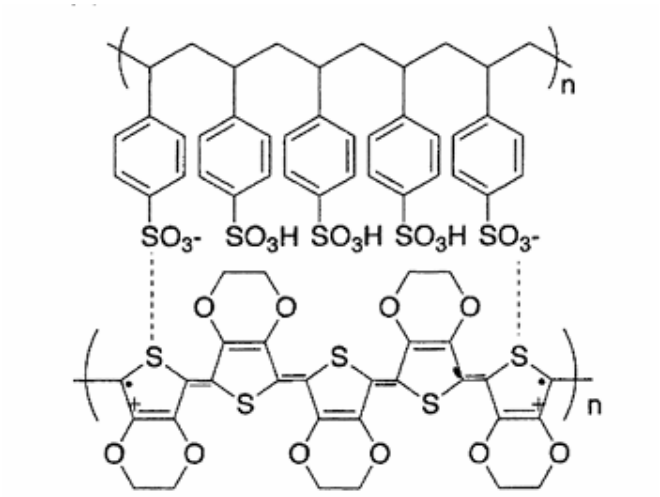

Figure 16: Structure of Poly (3,4-ethylenedioxythiophen)/polystyrene sulfonic acid (PEDOT:PSS) [39]

As PEDOT is an insoluble polymer, it is combined with polystyrene sulfonic acid (PSS) by polymerizing ethylene dioxythiophene with a water dispersible polyelectrolyte like PSS to make it solution processable. The resulting PEDOT:PSS is dark blue dispersion in water which has found a large number of industrial applications. This solution can be later used for making thin films by spin coating or dip coating and is baked at high temperatures to drive off water molecules. These films maintain their

conductivity even when heated in air for over 1000 hrs. For the fabrication of the solar cells in this study, PEDOT/PSS was obtained from Baytron P and used as received.

3.3 DNA-CTMA complex

As discussed earlier, DNA is a polar molecule with a negatively charged phosphate group on the backbone counter balanced by a positively charged sodium cation, and is only soluble in water. Figure 17 shows the picture of salmon DNA which has thread like appearance. In making solar cell devices, hydrophilic nature of the material is less desired and so DNA was treated with hexadecyl trimethyl ammonium chloride (CTMA) having a molecular formula, $CH_3(CH_2)_{15}N(Cl)(CH_3)_3$. CTMA has a positive charge on the nitrogen counter balanced by negatively charged chlorine. By mixing aqueous solution of DNA into aqueous solution of CTMA, ion exchange reaction occurs replacing ionically bonded Na ions on the DNA with the CTMA and eliminating NaCl as shown in Figure 18. The resulting DNA-CTMA precipitate is water insoluble and soluble in organic solvents like ethanol, methanol, and butanol. Butanol was the solvent used for DNA-CTMA as its boiling point is 118 °C, which helps in slow evaporation while spin coating and produce uniform film.

Figure 17: Salmon DNA [40]

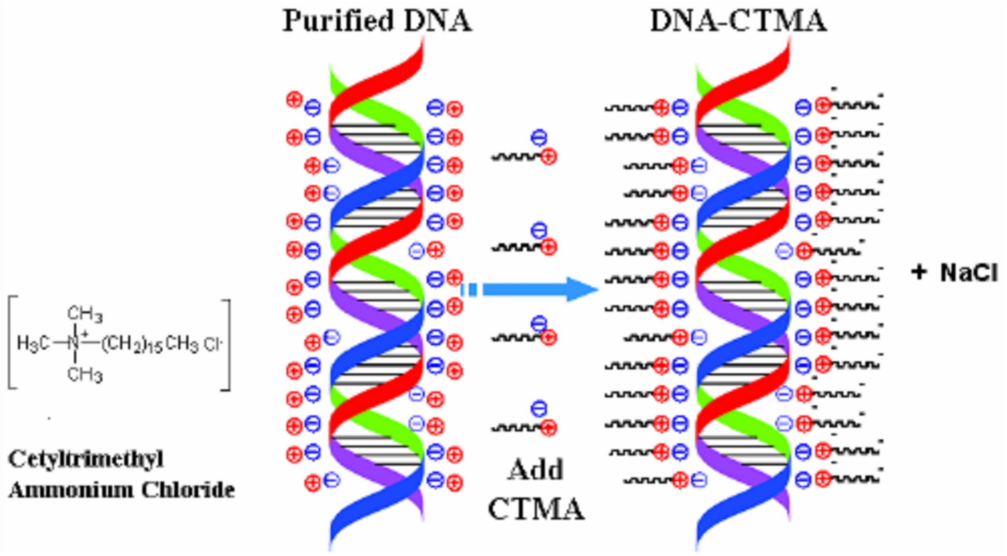

Figure 18: Ion exchange reaction to synthesize DNA-CTMA complex [41].

Figure 19: (a) Vacuum filtration unit, (b) DNA-CTMA complex after drying

DNA was obtained from Sigma Aldrich, which has molecular weight (MW) of $1.5x10^6$ g/mol or 2000 base pairs. CTMA was purchased form FLUKA chemicals and has a MW of 319.20 g/mol. The procedure to form the DNA complex was followed

from literature [42]. Initially equal wt % of DNA and CTMA was dissolved in 35 ml distilled water separately. To dissolve DNA the solution was stirred at room temperature with a star shaped magnetic stir bar for about 2 hours. After dissolution, the DNA solution was added slowly to CTMA solution while stirring the mixture as it was added. As soon as it was added, the solution formed precipitates. This solution was stirred for an additional 4 hrs at room temperature. This mixture was later vacuum filtered and dried in oven at 40^{o}C and stored in a desiccator for later use (Figure 19). DNA-CTMA is transparent in the visible spectrum, which makes it appropriate to be used as an optoelectronic material where transparency is necessary. Also, DNA complex layer is reported to show good mechanical properties as per thermogravimetric analysis (TGA) and dynamic mechanical analysis (DMA) [43].

3.4 Poly(3-hexylthiophene)

Polythiophenes are formed by the polymerization of thiophene monomer, a sulfur heterocycle. They belong to a class of polymers made up of alternate single and double C-C bond and is an example for linear pi-conjugated systems. These polymers show conducting behavior when electrons are added or removed from the conjugated pi-orbitals. Polythiophenes are of increasing interest because of the combination of electronic properties, environmental stability and their structural properties [44, 45]. Polythiophene is made soluble in organic solvents by the alkyl substitution (R) of the thiophene ring and the solubility increases with increasing the chain length of the substituent. The head and tail are the two connectivities of the thiophene ring at carbon-

2 and carbon-5 positions respectively. Figure 20 shows the two constitutional isomers, head-to-tail and head-to-head arrangements

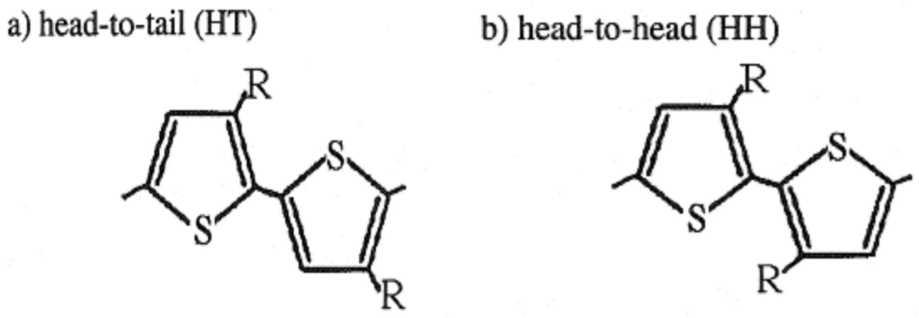

Figure 20: Structure of HT and HH or TT arrangement [46]

In this work, regioregular poly[3-hexylthiophene-2,5-diyl] from Sigma Aldrich was used as obtained without further purification. The regioregular structure has Head-to- Tail arrangement [46] and rod like conformation which results in improved conductivity, optical non linearity and magnetic properties [47].

3.5 Fullerenes

Buckminster fullerene (C_{60}) is the widely used electron acceptor because of its high electron mobility. The solubility of C_{60} is limited in many solvents and hence it is modified to PCBM ([6,6]-phenyl C_{61} butyric acid methyl ester), which has good solubility in many organic solvents like chloroform, chlorobenzene, etc.. The organic solar cells made using PCBM as electron acceptor has shown highest PCE of about 6.5% [26]. In this experiment, the PCBM used was obtained from Solenne B.V [48] and used as it is without further purification.

3.6 Device Fabrication

3.6.1 Preparing ITO glass substrates as anodes

Indium tin oxide (ITO) is the widely used transparent electrode in photovoltaic devices because of its transparency and low resistivity. ITO deposited glass sheets were obtained from Photran. The resistivity was 10-19 ohm/sq. Firstly, ITO was patterned to 1 inch x 1 inch using diamond tip cutter and cleaned with soap water. Then it was cleaned in an ultrasonic bath using organic solvents, toluene, acetone and isopropanol sequentially for 20 minutes each. The substrates were then blow dried with nitrogen gas and stored in tin boxes for later use.

3.6.2 DNA-CTMA and PEDOT/PSS as a hole transport layer

Poly(3,4-ethylenedioxythiophene):polystyrensulfonate (PEDOT/PSS), is the widely used hole transporting material in light-emitting diodes and photovoltaic applications. This material not only acts as hole acceptor but is also known to planarize the rough surface of ITO and also to improve the adhesion of other polymer layers. In this study, DNA-CTMA is used as a hole transporting material and compared with devices fabricated using PEDOT/PSS.

The PEDOT/PSS used in this study is Baytron-P (Bayer Corp., Germany). It is an aqueous dispersion of conducting polymer. PEDOT was spin coated on top of ITO deposited glass at 1500 rpm and was annealed at 95 °C for 5 minutes. Upon annealing, it formed a transparent blue film. Spin coating and annealing was carried out inside argon filled glove box.

DNA-CTMA complex formed by precipitating aqueous solutions of DNA and CTMA is used. 0.122g of DNA-CTMA complex was dissolved in 3ml of butanol in a brown bottle and stirred for about 19 hrs without heating. The solution is filtered using Whatman filter paper and spin cast at 1500 rpm and annealed at 40 °C for 5 mins.

3.6.3 PCBM-P3HT as Active layer

Various batches were made using P3HT-PCBM in different blend compositions using chloroform and chlorobenzene as the solvent. The polymers P3HT and PCBM were dissolved in organic solvent chloroform in different ratios of 1:1, 1:2 and 2:1 wt. %, having a concentration of 25g/litre. The different ratios are used to study the morphology of the cells. The polymers were weighed to a single brown bottle and the solvent chloroform was used and a magnetic stir bar was added. The solution was stirred for about 17hrs without heating and filtered using Whatman filter paper. The solution is spin-cast at 1500 rpm and annealed at 100 °C for 40, 30, 20, 10 and 5 minutes. All process steps from stirring to annealing is carried out inside high-purity argon filled glove box.

3.6.4 Spin coating

Spin coating is the deposition technique used to fabricate the hole transport layer and the active layer. Two sets of devices were fabricated for each composition of the active layer. The first device had ITO coated glass on which DNA-CTMA solution is spin coated at 2000 rpm and baked for 5 mins at 40 °C (This was arbitrarily chosen). Next, the active layer i.e., solution of P3HT/PCBM in chloroform was deposited by spin coating at 1500 rpm and baked at 100 °C for different times, to see if there was any

change in morphology of the blend. The second device had DNA/CTMA replaced with PEDOT/PSS which is spin coated at 1500 rpm and baked at 100 °C for 5 minutes to drive off the water content in PEDOT/PSS and all the other layers were processed according to the first device. Lastly, for the cathode, Al was deposited by thermal evaporation.

3.7 Cyclic Voltammetry (CV)

Cyclic Voltammetry is carried out for thin film of DNA-CTMA to study its oxidation behavior. This oxidation signal is important to find out the HOMO (Highest Occupied Molecular Orbital) level of the DNA-CTMA. By knowing the HOMO of the DNA-CTMA and the bandgap, its LUMO (Lowest Unoccupied Molecular Orbital) level is extracted. These values obtained are used in the band alignment of the solar cell. Another technique used to extract the HOMO level of polymers is the Ultraviolet Photoelectron Spectroscopy wherein it measures the ionization energy of the atoms. Since this method needs to be performed in vacuum it is not as convenient and cost effective as Cyclic Voltammetry.

Cyclic Voltammetry is an electrochemical measurement used to study the redox properties of compounds. In CV, the voltage is varied in a solution and the current variation with regard to the voltage change is measured. The three-electrode chemical cell is the widely used method because it uses a reference electrode whose potential does not vary during the measurement. The schematic of the three electrode cell is shown in Figure 21.

It consists of the reference electrode, working electrode and the auxiliary electrode or the counter electrode. An electrolyte is dissolved in a solvent and used to ensure good conductivity. Lithium perchlorate was the electrolyte used in this study which was dissolved in the solvent acetonitrile. The commonly used electrodes are platinum, gold or glassy carbon. They can be chosen from static or rotating type wherein rotation causes convection and eliminates the diffusion process. In this work, platinum was the electrode chosen for the counter electrode.

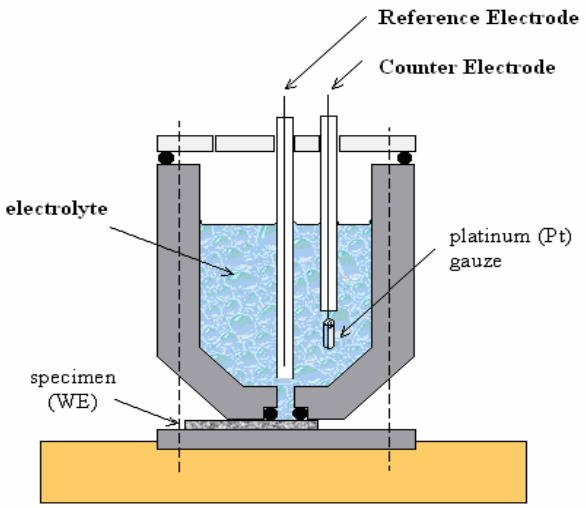

Figure 21: Schematic of three electrode electrochemical cell [49]

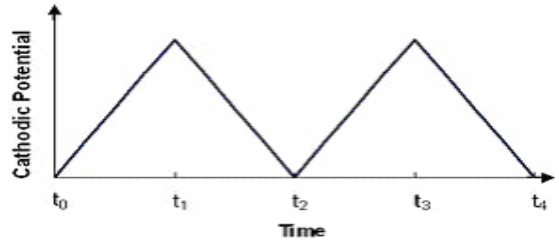

Figure 22: Cyclic voltammetry potential waveform [50]

In CV, the direction of the potential is reversed after scanning in the forward direction and the waveform obtained is of the form of an isosceles triangle. Figure 22 shows the CV waveform in which electrode potential follows a linearly increasing potential versus time. Scan rate is defined as rate of change of potential with respect to time. The advantage of CV is that the reaction that occurred in the forward scan can be probed again in the reverse scan.

In CV, the potential is measured between the working electrode and the reference electrode and the current is measured between the working electrode and the counter electrode. This is represented as a plot of current (I) versus voltage (V). A typical cyclic voltammogram is shown in Figure 23.

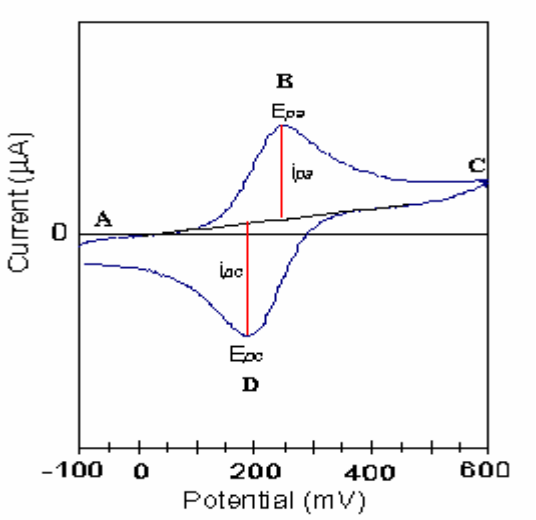

Figure 23: Typical Cyclic Voltammogram [51]

At the start of the experiment, the solution contains only the reduced form of the material (R). At the initial potential, there is no net conversion of R into oxidized form O, as the potential is lower than the redox potential which is represented as point A. As

the potential changes and reaches the redox potential, there is an exponential increase in current with respect to the potential which is the anodic current. At this point there is conversion of R into O and there is concentration gradients developed for R and O, where diffusion occurs between these concentration gradients.

At point B which represents the anodic peak the redox potential is very positive and for any R reaching the electrode surface, it is readily oxidized to O. At this point the current depends on the rate of mass transfer to the surface of the electrode which results in an asymmetric shape of the peak. The current starts to decrease as the concentration of the analyte is depleted near the surface of the electrode.

At point C, the applied potential is reversed and we see that the current decays until the potential is close to the redox potential. At this point, we see the cathodic current caused by the reduction of O to R which produces a cathodic peak at point D. The current produced in this scan has opposite polarity from the forward scan. Usually, the shape of the oxidation peak and the reduction peak is similar. Thus, CV is a powerful tool to obtain information regarding redox potentials, to detect the occurrence of chemical reactions and also for the evaluation of electron transfer kinetics.

In this study, CV of DNA-CTMA thin films were carried out for the first time using Lithium perchlorate and acetonitrile electrolyte. A small signal of the oxidation was observed. The onset of this oxidation was used to calculate the HOMO level of the DNA/CTMA. The Band gap of DNA-CTMA was extracted from the UV-absorption curve and later LUMO level of DNA-CTMA was calculated. These values were later used for the band alignment of the solar cell.

Several attempts were made to increase the signal of oxidation by varying the thickness of the film, by using ethanol and lithium perchlorate as an electrolyte, by using solution of DNA/CTMA and also changing the electrolyte to sodium phosphate buffer.

3.8 Characterization Techniques

3.8.1 I/V Measurements

The current versus voltage curves for the polymer PV cell was carried out under AM 1.0 condition using Keithley 2420 3A source measurement unit controlled by a computer program written in house. Projector lamp was purchased from GE lighting General and used to simulate AM 1.0, and crystalline silicon solar cell calibrated as AM 1.0 at NASA Glenn Research Center was used to calibrate our projector lamp. Figure 24 (a) shows the dark box used in this study and in Figure 24(b) we see the two point probe set up inside the dark box.

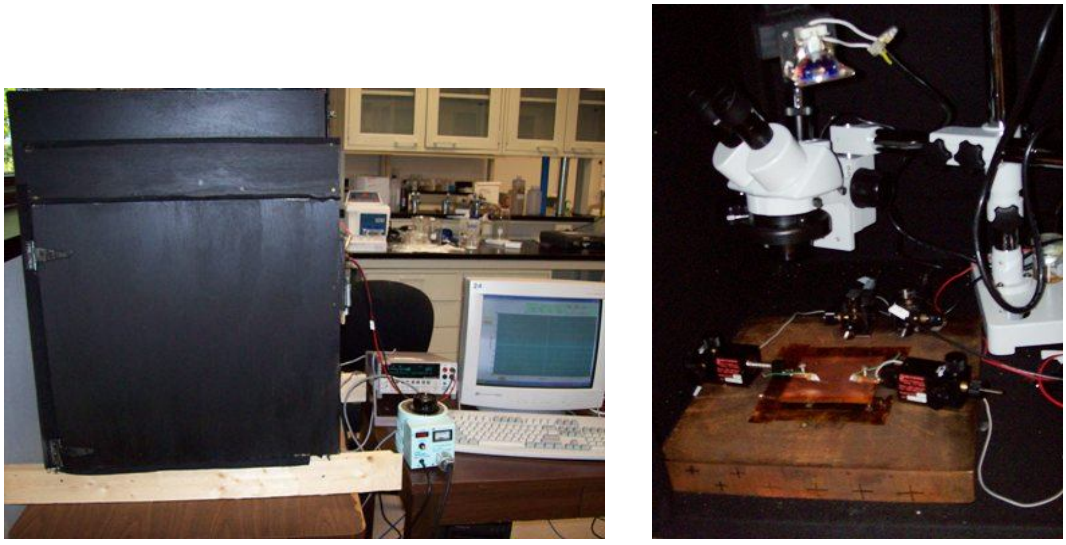

Figure 24: (a) Dark Box, sourcemeter and (b) Two point probe set up

3.8.2 Optical Microscopy

Optical Microscope was used to take surface images of all the spin coated films and also used to observe the device after top electrode application. The microscopic unit used for the characterization was Nikon Eclipse NE 600 (Figure 25).

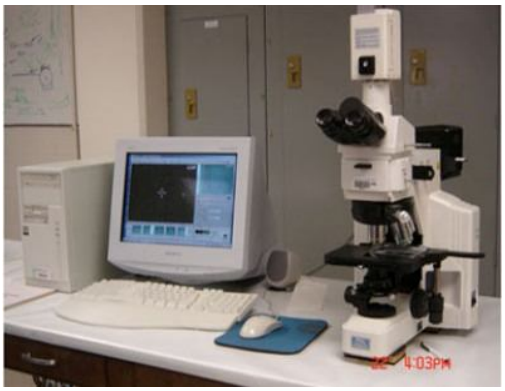

Figure 25: Optical microscope used for cell characterization.

3.8.3 Thickness Measurement

The thickness of the films deposited by spin coating was measured by Dektak IIA Profilometer (Figure 26). For the thickness measurement, a trench was formed on the film by fixing scotch tape and carefully removing the sample in a small area using the solvent which dissolves the polymer and later peeling the scotch tape.

Figure 26: Profilometer.

3.8.4 UV-Visible NIR spectroscopy

Spectroscopy is a branch of science in which light is used to study the structure of matter and used to carry out qualitative and quantitative analysis. It is also used for the identification of substances from the spectrum emitted or absorbed by the substances. In this study, absorbance and % transmittance was carried out using a Perkin Elmer UV-Visible-NIR Spectrometer Lambda 19 unit (Figure 27).

Figure 27: Perkin Elmer UV-Visible-NIR Spectroscopic unit.

3.8.5 Fluorescence Spectroscopy

In this technique, higher energy photons are used to excite a sample which will later emit photons in the lower energy. This is a very useful technique used in photovoltaic application and in light emitting devices. This provides information on the exciton dissociation in the active layer to form free charge carriers. The Fluorescence Spectroscopy unit used was Perkin Elmer Fluorescence Spectrophotometer 204-A (Figure 28).

Figure 28: Fluorescence Spectroscopy.

3.8.6 Fourier Transform Infrared Spectroscopy (FTIR)

FTIR is a measurement technique which captures the infrared spectra. This is used in this study to detect the signal from the CTMA attached to the DNA molecule. The FTIR used for characterization was Thermo FT-IR Nicolet-700 (Figure 29).

Figure 29: FTIR Unit.

3.8.7 Glove Box

The spin coating of the various layers of the bulk heterojunction solar cell was carried out inside Ar purged glove box. The glove box from LABCONCO was used and

the spin coater (Specialty Coating Systems, P6700) and the hot plate used in this experiment is shown in Figure 30.

Figure 30: (a) Argon purged Glove box (b) Spin coater and hot plate

CHAPTER 4

RESULTS AND DISCUSSIONS

In this section, the results obtained from different measurements like optical transmittance, infrared spectroscopy, cyclic voltammetry carried out on DNA complex layer to evaluate its use in photovoltaic device are discussed. This is followed by the presentation of optical data, transmittance and the photoluminescence results obtained from the P3HT-PCBM blend films. Finally the different top electrode materials used is highlighted followed by the discussion of the solar cell measurements carried out on the devices.

4.1 Transmittance of DNA-CTMA thin film

The optical absorption plays a key role when using DNA-CTMA as a hole transport layer in bulk heterojunction polymer solar cells. UV-Visible-NIR spectroscopy was carried out for DNA-CTMA thin film on quartz substrate. From the graph (Figure 31), DNA-CTMA film shows 90% transmittance in the visible region and the infrared (from 400 nm to 1000 nm) and shows an absorption peak at 260 nm. The hole transport layer does not contribute to absorption of light since the absorber layer is used for this purpose. A hole transport layer should be optically transparent so that more light can reach the absorber layer.

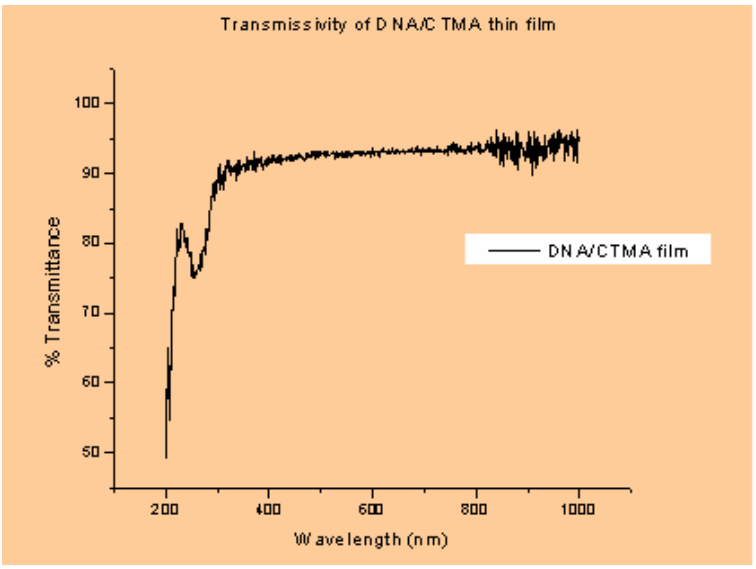

Figure 31: Optical transmittance of DNA-CTMA thin film on quartz substrate

4.2 Inductively Coupled Plasma Mass Spectroscopy (ICPMS)

ICPMS was carried out to find the amount of sodium present in DNA-CTMA complex. This was done outside the campus at West Coast Analytical Service (WCAS). While making DNA-CTMA complex, after filtering the precipitate, about one liter of distilled water was run through to remove the unwanted sodium. From the result of this experiment for DNA-CTMA complex, 13.2 μg/g of Sodium was detected. The amount of sodium in DNA before reacting with CTMA was found to be 0.0192g. After forming DNA-CTMA, the amount of sodium present is 5.225 μg, which is about 0.02 wt% of the initial amount of sodium in DNA and this confirms most sodium is replaced with CTMA.

4.3 Fourier Transform Infrared Spectroscopy

FTIR spectroscopy is a well known technique for structural analysis of polymers and is used to investigate the synthesis of DNA-CTMA complex. FTIR was carried out

for DNA and DNA-CTMA film formed on silicon substrate by spin coating. Two vibrational signals corresponding to CTMA is seen in Figure 32 in which the peak at 2887 cm^{-1} and 2961 cm^{-1} corresponds to -(CH_2)- signal and -(CH_3)- signal as compared to the literature values of 2852 cm^{-1} and 2950 cm^{-1} respectively [52]. Several peaks are observed which correspond to the vibration of DNA molecules. The following table (Table 1) lists the different frequencies of vibration bands for DNA.

Table 1: List of frequencies of vibrational bands of DNA and CTMA [53].

Wavenumber (cm^{-1})	Associated signal
970	Sugar-phosphodiester signal
1090	Symmetric phosphate stretching
1225	Asymmetric phosphate stretching
3187	Symmetric stretching of the NH group of the bases
1328	Aromatic amine stretching
1715	Guanine-Thymine carbonyl stretching
2887	-(CH_2)- signal from CTMA
2961	-(CH_3)- signal from CTMA

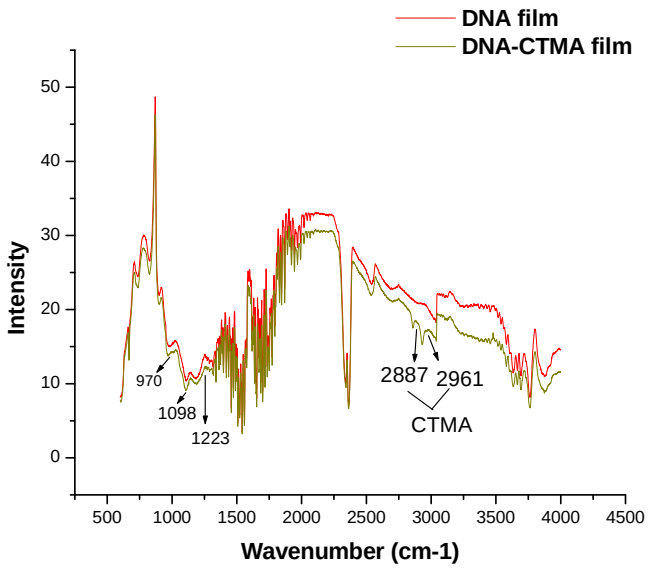

Figure 32: FTIR spectroscopy of DNA and DNA-CTMA thin film

4.4 Cyclic Voltammetry of DNA-CTMA film

In this work, the CV of DNA-CTMA is carried out to find the signal of oxidation. Thin film of DNA-CTMA on ITO electrode is formed by spin coating and was used for the measurement. The electrolyte used is lithium perchlorate which is dissolved in acetonitrile. Acetonitrile does not dissolve DNA-CTMA film.

CV scan was carried out on DNA-CTMA film as shown in Figure 33. A peak is observed which initializes at 533mV and is the oxidation peak with a maximum position at 793mV. Similar peak was observed in the literature which is ascribed to the oxidation of DNA through the guanine bases [54], where anodic process occurring in the range of +700 to +800mV due to guanine residues. Also, Guanine oxidizes easily compared to the other bases and is attacked by the oxidizing agents readily. From the

figure, the onset of oxidation is taken to be 533mV and used to calculate the HOMO level of the DNA-CTMA.

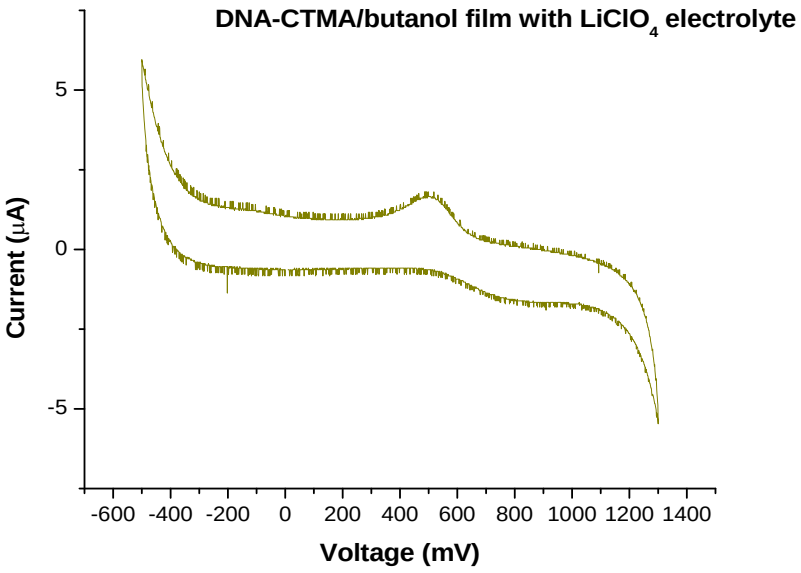

Figure 33: CV of DNA-CTMA film.

Figure 34 shows the CV measurement carried out for bare ITO electrode. This was carried out to know if ITO is contributing to any peaks in the potential range used to scan the DNA-CTMA. In order to increase the intensity of oxidation peak observed in DNA-CTMA film, several extra CV measurement were carried out by changing parameters like scan rate, electrolyte solvent and using DNA-CTMA solution. But these did not enhance the intensity of the oxidation current. In fact, acetonitrile does not dissolve DNA-CTMA well and it is thought that only limited number of ions in acetonitrile reach guanines.

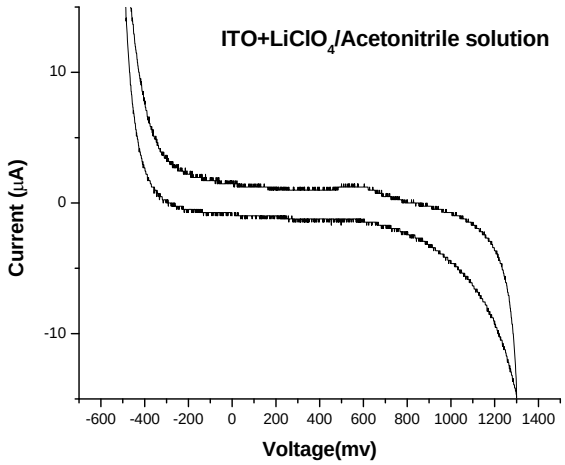

Figure 34: CV of ITO electrode using Lithium perchlorate/Acetonitrile electrolyte.

4.4.1 HOMO and LUMO level of DNA/CTMA film

To calculate HOMO and LUMO levels, the band gap of DNA-CTMA is determined first from the transmittance data (Figure 35) and it is about 4.1 eV.

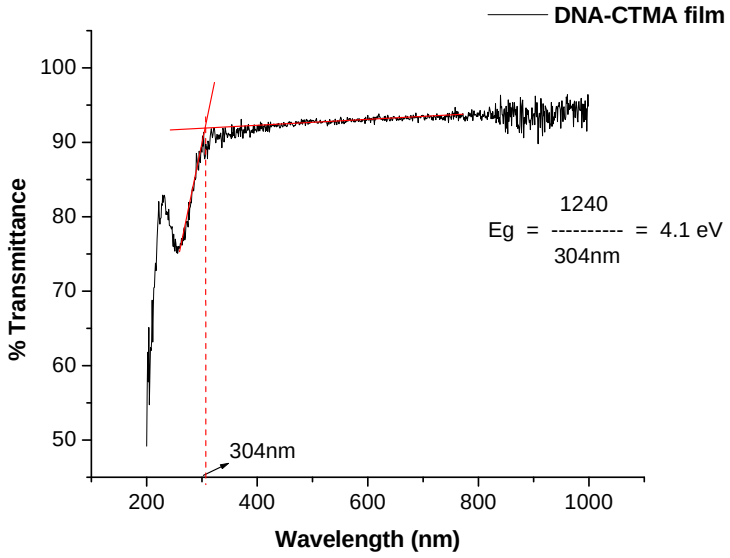

Figure 35: Extrapolating the bandgap from the transmittance data.

The equation 1 shown below is used to find the HOMO level of DNA complex layer [55]. In the equation, FC stands for ferrocence (FC), Ref. stands for reference and it is found to be 0.13 V for the CV set up used. The energy values of the highest occupied molecular orbital (HOMO) for the synthesized polymers is reported as -4.8 eV using the ferrocence ion below the vacuum level.

$$E_{HOMO} = [-e\ (E_{OX,\ ONSET(VS.\ Ag/AgCl)} - E_{ONSET(FC\ VS.\ Ag/AgCl)\ Ref}] - 4.8\ eV \ldots\ldots (1)$$

$$= [-e\ (0.533\ V - 0.13\ V)] - 4.8\ eV$$

$$= -\ 5.203\ eV|vacuum$$

$$= 5.203\ eV$$

And,

$$E_{LUMO} = E_{HOMO} - E_g$$

$$= 5.203 - 4.1\ eV = 1.1\ eV$$

4.4.2 Band Alignment of the solar cell

Figure 36 compares the band alignment for the devices using conventional PEDOT-PSS (Fig 36a) and DNA-CTMA (Fig 36b) used as hole transport layer. From the figure, we see that the HOMO level of DNA-CTMA extracted from the cyclic voltammetry data obtained in this study is on par with the HOMO of the PEDOT-PSS with a value of about 5.2 eV. The LUMO level of DNA is 1.1 eV compared to the LUMO of PEDOT-PSS, 3.5 eV. This shows that DNA-CTMA prevents the back flow of electrons traveling from P3HT to ITO effectively compared to PEDOT-PSS.

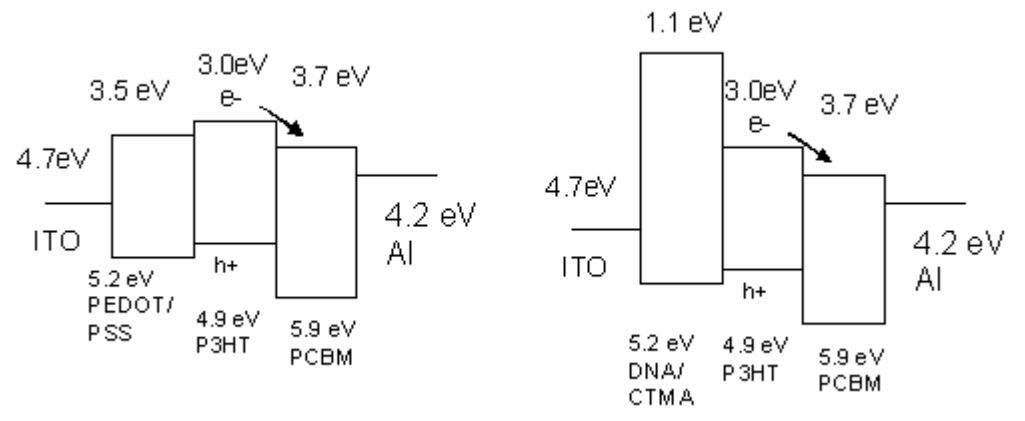

(a) (b)

Figure 36: Energy Band Diagram of bulk heterojunction solar cell using (a) PEDOT-PSS (b) DNA-CTMA as hole transport layer.

So far, the different characterization techniques carried out on DNA-CTMA was discussed. Now we shall look into the characterization methods used for P3HT-PCBM active layer deposited on different substrates like ITO, ITO+DNA-CTMA layer and ITO+PEDOT-PSS layer. First the optical images of the active layer are presented followed by the transmittance data and then the results obtained from the fluorescence measurements are presented. Finally the different top electrode materials used in this study are introduced followed by the discussion of results from the cell measurements..

4.5 Effect of solvent

Two different solvents chloroform and chlorobenzene is used to make the active layer films in this study. Chloroform was used as a solvent to fabricate cells from the start of the study. From the literature [7], it was found that the non-aromatic solvent prevents good contact between the polymers in the active layer and decrease solubility and hence we decided to try the aromatic solvent chlorobenzene. The experiments carried out using each solvent is discussed separately.

4.5.1 Chloroform as the solvent

In the making of a cell, P3HT-PCBM active layer was deposited on four different substrates namely glass/ITO, glass/ITO/DNA-CTMA, glass/ITO/PEDOT-PSS, and bare quartz substrates. Quartz substrates were used because quartz is transparent in the visible spectrum and part of UV spectrum and therefore used to characterize the transmittance of the active layer. Cells were fabricated by spin coating and were annealed at different temperatures.

4.5.1.1 Time Effect

Time effect corresponds to the different annealing time used for baking the films formed by spin coating. We observed that the samples baked for less time like 5 minutes showed very little PCBM molecules crystallizing to form needles in the active layer as shown in Figure 37(a) whereas the samples annealed for longer time like 1 hr showed increased number of needles formed in the active layer as shown in Figure 37(b).

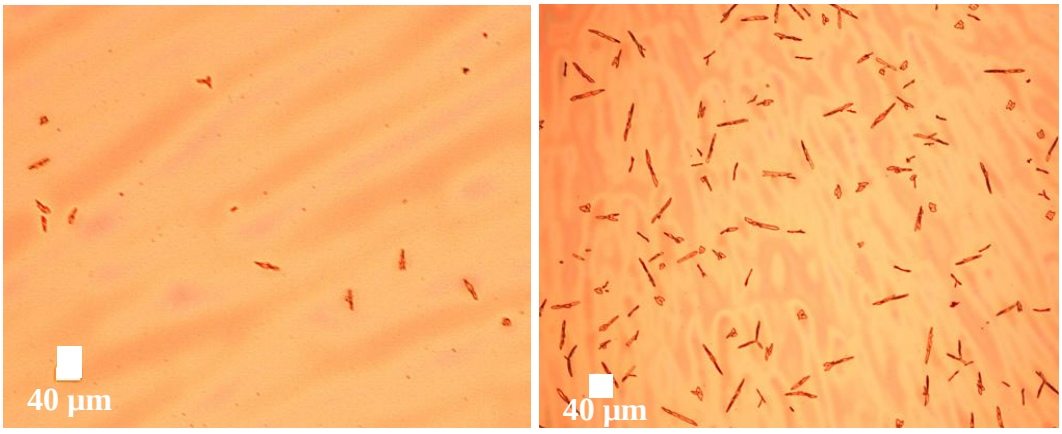

(a) (b)

Figure 37: Optical images of P3HT-PCBM (60-40) wt% spin coated on DNA-CTMA thin film annealed at 100 °C for (a) 5minutes and for (b) 60minutes.

4.5.1.2 Composition Effect

It was observed that the change in composition of the active layer greatly affects the formation of needles. It was found that with increasing the amount of PCBM in the blend, the number of needles and the size of the needles also increased. In Figure 38(a), when the PCBM content is in the ratio of 1:1 wt%, there is few crystallites formed whereas in Figure 38(b) the PCBM is doubled (1:2 wt%), which shows a network of needles formed in the active layer.

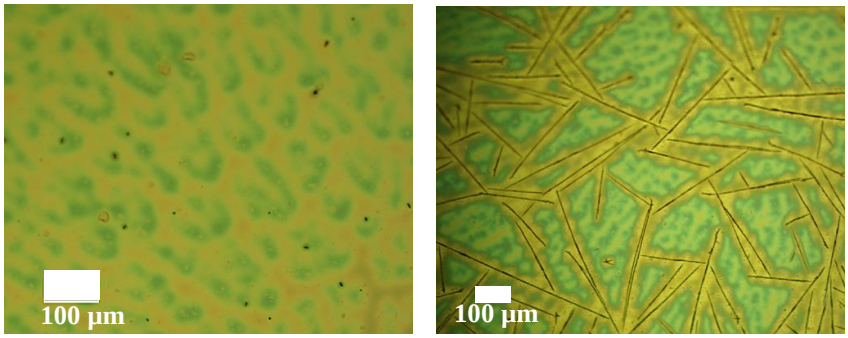

(a) (b)

Figure 38: Optical images of (a) P3HT-PCBM (50-50) wt% (b) P3HT-PCBM (33-66) wt%, spin coated on PEDOT-PSS layer and annealed at 100 °C for 40minutes.

4.5.1.3 Substrate Effect

The sample spin coated on ITO without using DNA-CTMA thin film shown in Figure 39 (a) was annealed at 100°C for 60 minutes and did not show large difference in needle formation but slight increase in number of needles was observed in the presence of DNA-CTMA film annealed for the same time as in Figure 39(b).

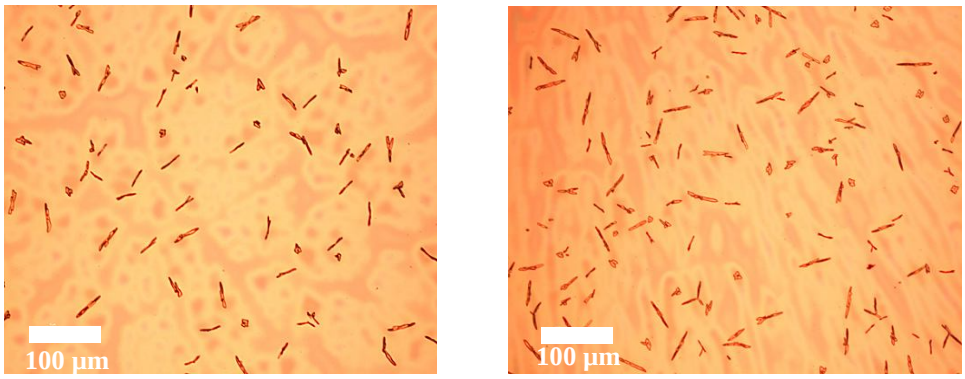

(a) (b)

Figure 39: Optical image of P3HT-PCBM (60-40) wt% spin coated (a) on ITO, (b) DNA-CTMA, annealed at 100 °C for 60minutes.

The Figure 40 below shows the optical image of P3HT-PCBM (33-66) wt % spin coated on (a) DNA-CTMA layer and on (b) PEDOT-PSS layer. It was found that the film on PEDOT-PSS layer showed very large number of needless formed in the active layer compared to film on DNA-CTMA layer. Since needles are not preferred as they are increase the exciton recombination at those sites, having DNA-CTMA is an advantage compared to PEDOT-PSS.

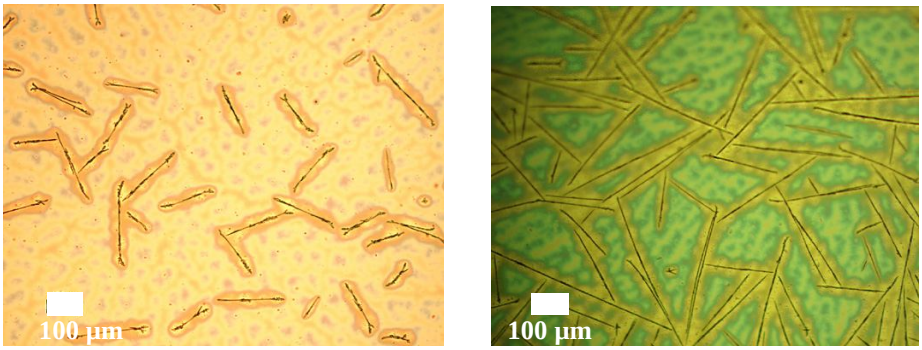

(a) (b)

Figure 40: Optical images of P3HT-PCBM (33-66) wt% spin coated on (a) DNA-CTMA layer (b) PEDOT-PSS layer, annealed at 100 °C for 40minutes.

4.5.2 Chlorobenzene as the solvent

The use of chlorobenzene as the solvent is said to increase the solubility of the active layer when compared to the chloroform based films. In this study when chlorobenzene was used as a solvent, the amount of needles formed in the active layer was very high compared to the films formed using chloroform. One of the reasons could be because the boiling point of chlorobenzene is 131ºC compared to chloroform which is 61.2 ºC. So in case of chlorobenzene, the solvent is present for longer duration which allows PCBM molecules to crystallize more.

4.5.2.1 Time Effect

In case of chlorobenzene, the samples annealed for short duration and those annealed for longer duration of time, both showed network of needles formed in the active layer and there was slight increase in network of needles from 5 minutes to 40 minutes of annealing time as shown in Figure 41.

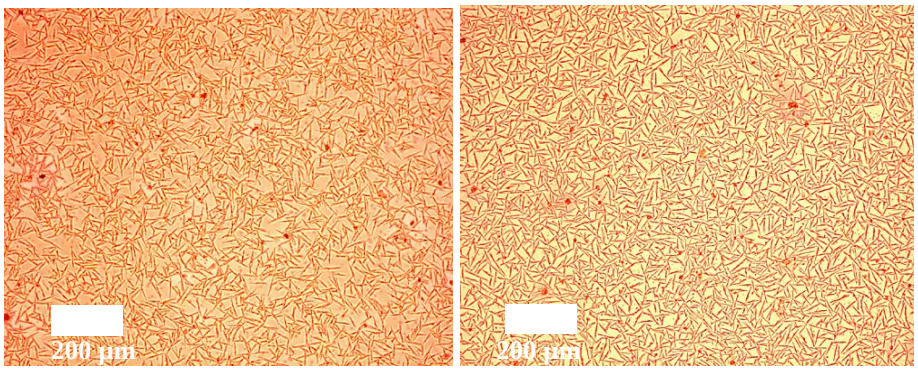

(a) (b)

Figure 41: Optical images of P3HT-PCBM (33-66) wt % spin coated on DNA-CTMA layer, annealed at 100 °C for (a) 5 minutes and (b) 40minutes.

4.5.2.2 Composition Effect

As discussed earlier, with increasing the concentration of PCBM, the needle formation also increased using chloroform solvent. In case of chlorobenzene, the amount of needles formed in the active layer was very high compared to the films formed using chloroform. Figure 42 below shows the optical images for 1:1 wt % P3HT-PCBM and 1:2 wt% P3HT-PCBM wherein we see large number of needles formed in 1:1 ratio which increases further to form a network of needles with increasing PCBM content.

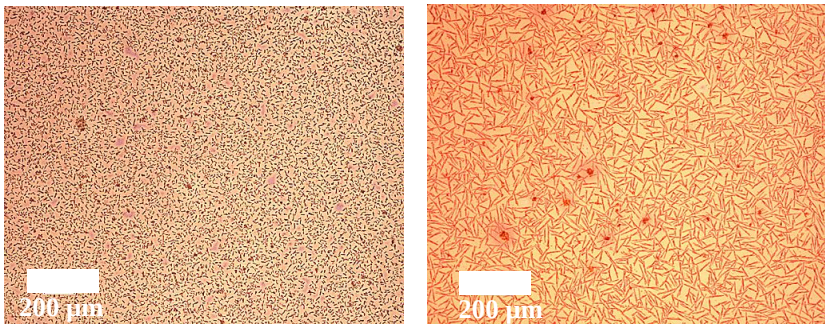

(a) (b)

Figure 42: Optical images of (a) P3HT-PCBM (50-50) wt% (b) P3HT-PCBM (33-66) wt% spin coated on DNA-CTMA layer, annealed at 100 °C for 30 minutes

4.5.2.3 Substrate effect

Figure 43 below shows the optical image of P3HT-PCBM (33-66) wt % spin coated on on (a) ITO and (b) DNA-CTMA layer. It was found that the film on DNA-CTMA layer showed longer needles formed in the active layer compared to film on ITO substrate wherein, the needles are smaller.

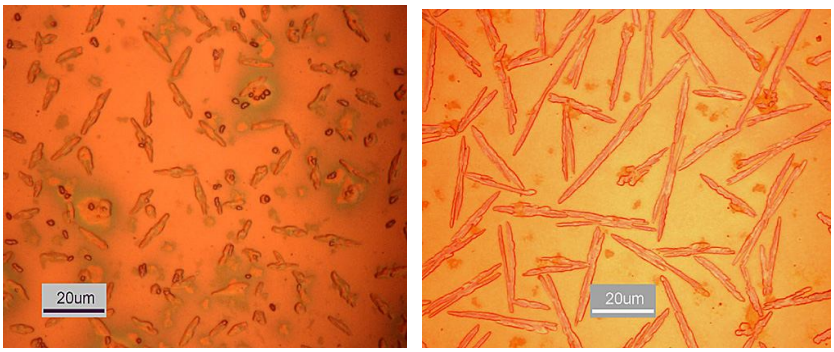

(a) (b)

Figure 43 : Optical images of P3HT-PCBM (33-66) wt% spin coated on (a) ITO (b) DNA-CTMA layer, annealed at 100 °C for 30 minutes (Scale bar: 20 µm)

4.6 Optical Absorption/Transmission

Optical absorption/transmission study is carried out to find the amount of light absorbed/transmitted by the individual polymers. Each polymer requires different absorption characteristics while using in polymer solar cells. As discussed earlier for using a polymer as a hole transport layer, the material should possess good optical transmittance so that more light can reach the absorber layer. For polymer like P3HT, to be used as an absorber layer, it should have good absorption in a wide spectrum of light so that more photons can be captured and in turn generates more photocurrent.

Thin Films were made using individual polymers like DNA-CTMA, P3HT, PCBM, and PEDOT-PSS and the optical transmittance studies were carried out. The following plot (Figure 44) shows the transmittance data in which P3HT has a wide absorption band from 350nm to 650nm which is responsible for 80% absorption of light in the visible spectrum. In case of PCBM, absorption peaks are observed at 336nm and 265nm where most of the photons are captured by PCBM. While comparing DNA-CTMA and PEDOT-PSS film we see that the % transmittance in DNA-CTMA film is

90% whereas PEDOT-PSS has a wide absorption band from 300-650nm. This shows that if DNA-CTMA is used as a hole transport layer, more light reaches the active layer when compared with PEDOT-PSS.

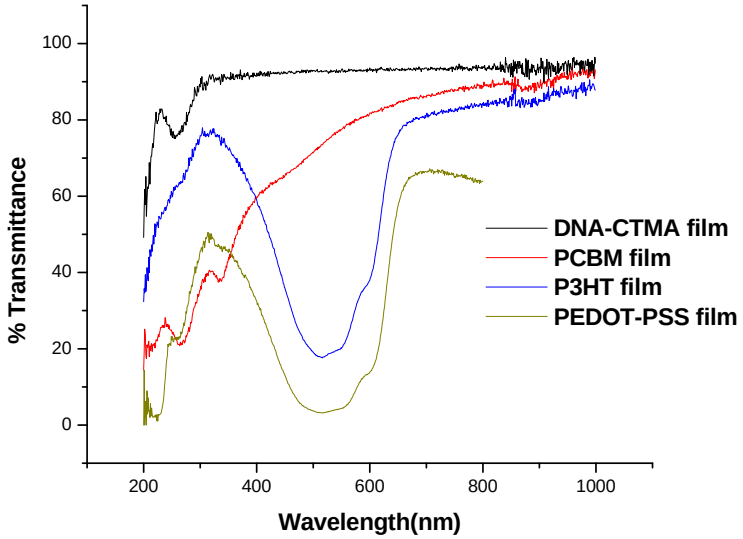

Figure 44: Transmittance curves for individual films of PCBM, P3HT and DNA-CTMA.

The following Figure 45 shows the transmittance curves obtained for P3HT-PCBM (60-40 wt %) formed on DNA-CTMA layer which was annealed at 100°C for different annealing time. We see that, there is not much difference observed in absorption of P3HT and PCBM when annealing is increased from 5 to 10 minutes because the number of PCBM needles formed in these two samples was comparable and there were no drastic changes occurring in the polymer matrix. When the annealing time was increased further to 60 minutes, the absorbance of PCBM decreases by ~15% (Fig 45). This could be because of the increasing number of PCBM needles with

increasing annealing time which might have reduced the absorption from PCBM molecules.

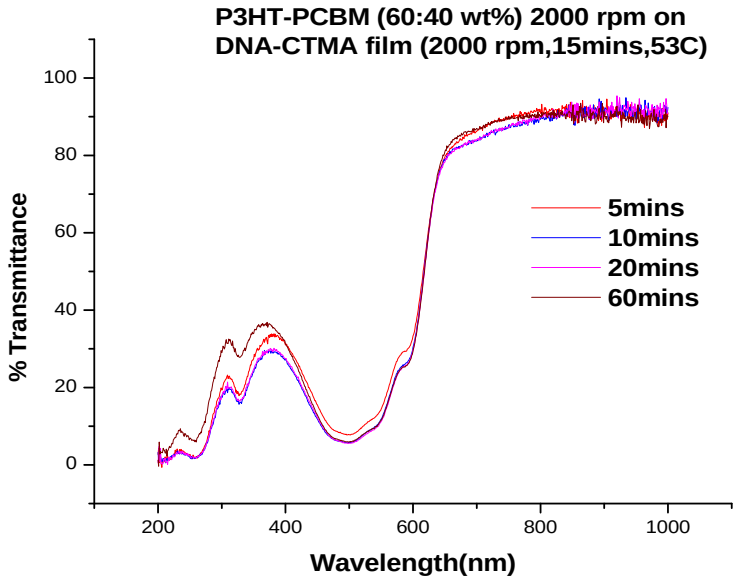

Figure 45: Transmittance data of P3HT-PCBM (60-40) wt% spin coated on DNA-CTMA thin film annealed for different times at 100 °C.

Figures 46-48 show the % transmittance data carried out for films of P3HT-PCBM in different ratios namely 66-33 wt%, 50-50 wt% and 33-66 wt%. All these films are spin cast on DNA-CTMA film and PEDOT-PSS film at 1500 rpm and annealed at 100 °C for 5 minutes and 40 minutes.

The absorber layer (P3HT-PCBM) has to absorb more light so that more charge carriers are generated, in turn increasing the photocurrent. For example, if the absorption of light by active layer is limited to visible spectrum, then the photons coming from the infrared and the ultraviolet spectrum are lost without absorption, thereby reducing the free carrier formation and the current. When optical transmittance

is carried out for various blend compositions, the optimum absorption occurring in entire light spectrum can be found. This helps us to choose the right composition for the active layer. From Figure 46 for P3HT-PCBM (66-33 wt %), there is high absorption observed in the visible region occurring from P3HT. Also we do not see much difference in the absorption for P3HT while spin coating on DNA-CTMA (D-C) and PEDOT-PSS (P-P) layers, which implies that the substrate effect is minimal. At 250 nm PEDOT-PSS layer shows less transmittance than DNA-CTMA layer. Also from 650-800 nm active layer on DNA-CTMA shows 90% transmittance than PEDOT-PSS which shows ~65% transmittance. By comparing the Figures 46, 47 and 48 we see that the intensity of absorption from P3HT is high in the blend P3HT-PCBM (66-33 wt %) due to high amount of P3HT and decreases with increasing amount of PCBM as seen in P3HT-PCBM (50-50 wt%) and P3HT-PCBM (33-66 wt%) films. The blend with P3HT-PCBM (50-50 wt %) and P3HT-PCBM (33-66 wt%) shows good absorption over the entire spectrum compared to P3HT-PCBM (33-66 wt %) which has high absorption in a limited wavelength range of 350nm to 650nm.

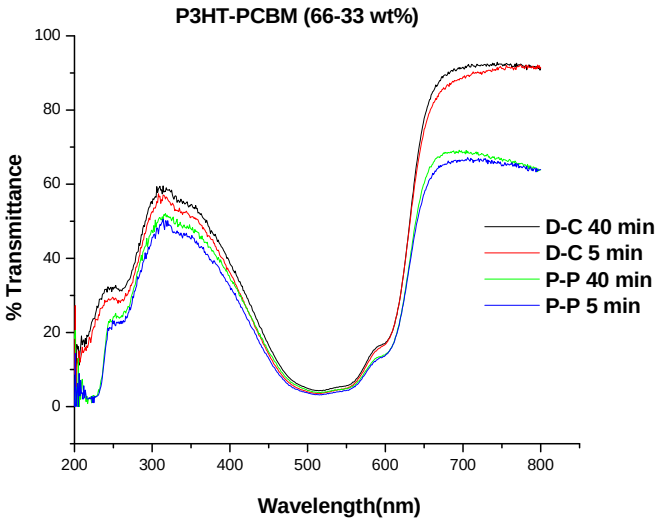

Figure 46: % Transmittance for P3HT-PCBM (66-33 wt%) spin coated on DNA-CTMA and PEDOT-PSS layer annealed at 100 °C for 40 and 5 minutes.

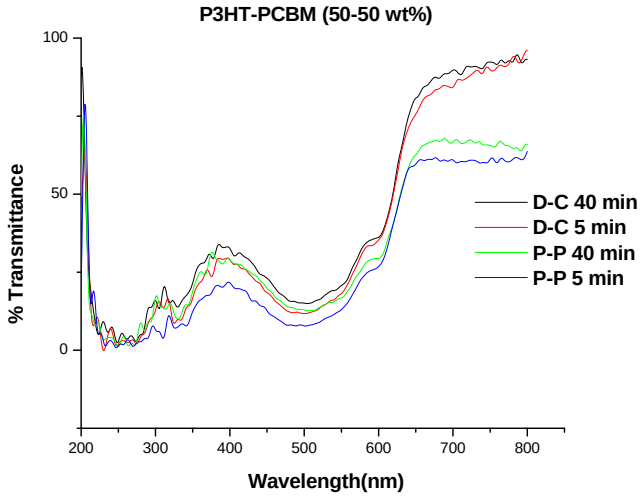

Figure 47: % Transmittance for P3HT-PCBM (50-50 wt%) spin coated on DNA-CTMA and PEDOT-PSS layer annealed at 100 °C for 5 and 40 minutes.

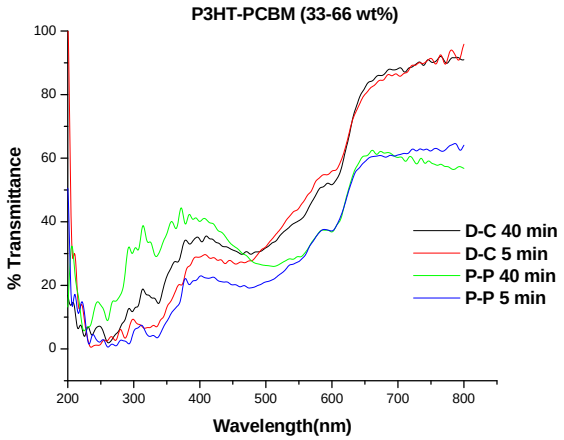

Figure 48: % Transmittance for P3HT-PCBM (33-66 wt%) spin coated on DNA-CTMA and PEDOT-PSS layer annealed at 100 °C for 5 and 40 minutes.

4.7 Fluorescence spectroscopy (FL)

FL is an important characterization technique which gives information about the exciton dissociation to form free charge carriers in the absorber layer (P3HT-PCBM). If FL quenching occurs in the absorber layer, it means excitons are dissociated to form free charge carriers which contribute to the current and hence the signal of fluorescence is low.

When fluorescence is carried out on pure polymer films like P3HT, a high fluorescence signal is obtained because there is no exciton dissociation due to the absence of the acceptor molecule like PCBM and hence exciton recombination is taking place, indicating that the polymer is pure without defects. If it has defects, then the excitons can undergo non-radiative recombination in those trap sites and reduce the fluorescence intensity thereby giving information on the purity of the polymer.

Fluorescence (Figure 49) of pure P3HT films formed by spin coating at 2000 rpm and annealed at 100 °C for various times of 5, 10, 20, 30 and 40 minutes were carried out. The sample baked for 5 minutes shows less fluorescence signal may be due to the presence of defects and as the annealing time is increased we see increase in the fluorescence intensity which indicates that the polymer chains are trying to form an ordered structure by reducing the number of defect sites. Another observation is that the film baked for 40 minutes shows less fluorescence signal compared to the 30 minutes baked sample. The result is not clear but one of the reasons could be that when baked for 30 minutes, it possesses the optimum arrangement of the P3HT chains without defects so high intensity signal is observed, which decreases with further annealing.

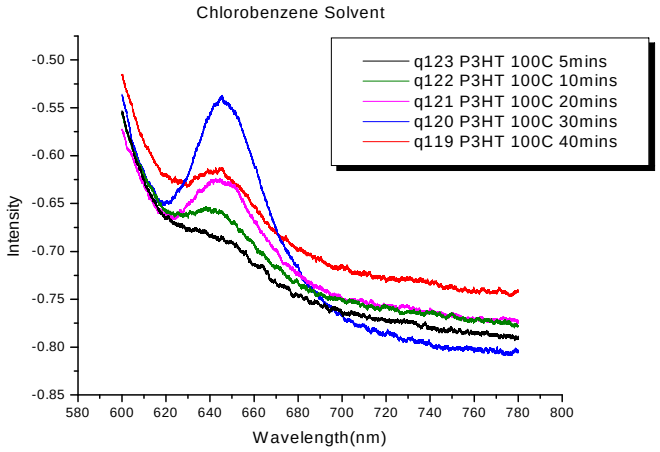

Figure 49: FL spectra for P3HT only films annealed at 100 °C for various time of 5, 10, 20, 30 and 40 minutes using chlorobenzene as the solvent.

When fluorescence is carried out for P3HT-PCBM blend, we expect the intensity of the fluorescence signal to be low. This is because when light is absorbed by P3HT, it creates excitons. These excitons generated in the P3HT molecule diffuse to the

interface of the P3HT-PCBM blend and dissociate to form free charge carriers thereby contributing to the current. If excitons generated in P3HT molecule recombines to give out light, they are not contributing to the current and we see a large fluorescence signal. To confirm this, the fluorescence of the blend films was carried out.

Pure P3HT films (Figure 49) were compared with the FL spectra (Figures 50, 51 and 52) of P3HT-PCBM blend. The comparison among figures indicates a drop in intensity of FL peak and confirms that when P3HT is blended with PCBM, the excitons formed are dissociating without recombination of electrons and holes, thereby contributing to the current.

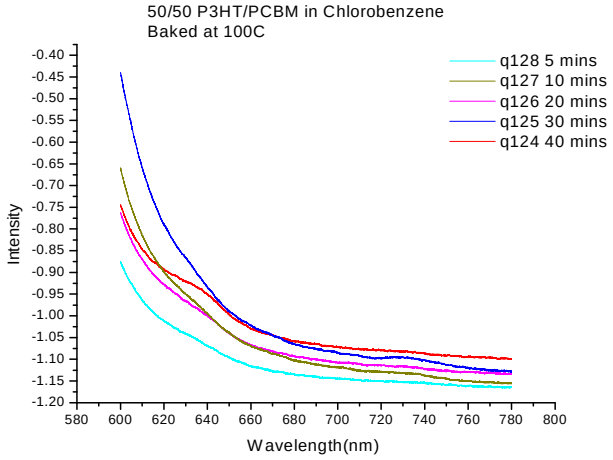

Figure 50: FL spectra for P3HT-PCBM (50-50 wt%) films annealed at 100 °C for various time of 5, 10, 20, 30 and 40 minutes using chlorobenzene as the solvent.

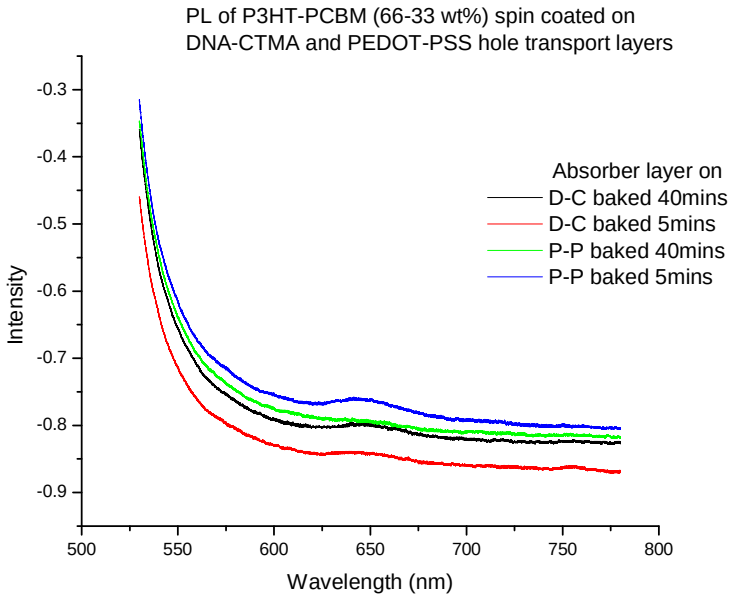

Figure 51: FL spectra for P3HT-PCBM (66-33 wt%) films spin coated on DNA-CTMA and PEDOT-PSS hole transport layers and annealed at 100 °C for 5 and 40 minutes using chloroform as the solvent.

Figure 52 shows FL spectra for P3HT-PCBM (60-40) wt% spin coated on DNA-CTMA thin film and annealed for different times at 100 °C. In the figure, FL is quenched, which is an indication that electrons and holes are not recombining to emit light but they are dissociating and contributing to the number of free charge carriers. The films were excited at 450nm and scanned from 500nm to 780nm.

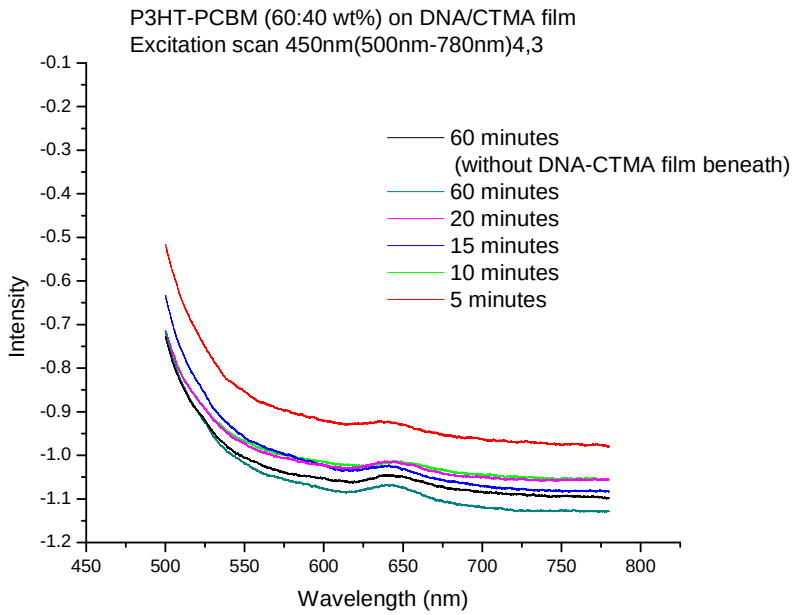

Figure 52: Photoluminescence spectra for P3HT-PCBM (60-40) wt% spin coated on DNA-CTMA thin film and annealed for different times at 100 °C

4.8 Top Electrode Materials

Several top contact materials like silver pastes (Premetek, 1228 & Alfa International Corporation E10-101), Ga-In Eutectic alloy (Aldrich, 495425), copper tape (SPI) and evaporated Al were tried and compared in order to study if painted (or printed) metal electrode can be used in real device architecture compared to the commonly used evaporated metal electrodes. The silver paste was applied by using the back end of the cotton swab. When silver paste (Premetek, 1228) was applied on top of P3HT-PCBM device, there was penetration of the solvent from the silver paste to the surrounding area and to the bottom electrode resulting in shunting. Figure 53 shows the solvent spreading to the film from the silver paste.

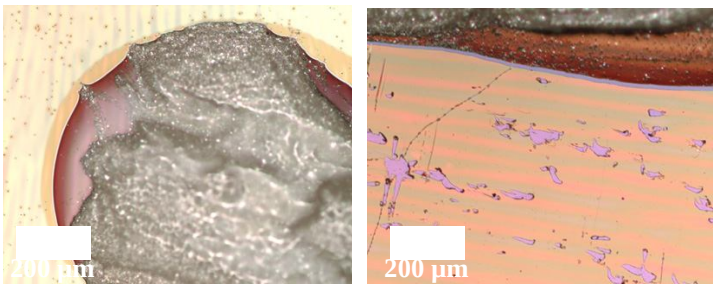

(a) (b)

Figure 53: Optical image of the silver paste used as the top contact.

Figures 54 (a) and (b) shows the use of Ga-In eutectic alloy as the top electrode which penetrated to the bottom electrode through the film causing shunting. This electrode was applied using the back end of the cotton swab. Fig 54 (a) is the front view and 54 (b) is the back view where we see some white marks which correspond to the Ga-In eutectic alloy reaching the bottom surface and reflecting light.

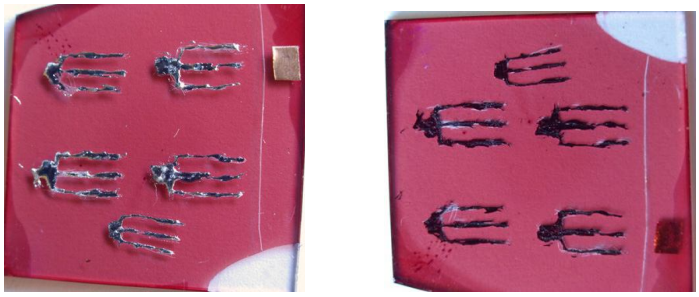

(a) (b)

Figure 54: Pictures showing (a) painted Gallium Indium Eutectic alloy - front view (b) painted Gallium Indium Eutectic alloy -back view, used as top electrode.

The use of copper tape as the top electrode did not show good results due to the poor contact between the film and the electrode. In order to prevent the damage from the solvent of the silver paste, silver paste (E10-101) which is solvent free was used in the experiment. In this case, we did not see any dissolution of the film or penetration of electrode to the bottom electrode. The sample is shown in Figure 55. Since this silver

paste was based on mixing equal quantities of silver paste and curing agent, and allowing 24 hrs to cure after application and to carry out the measurements. No photovoltage and very small photocurrent was obtained with this silver paste. Further study is needed to understand more about the paste.

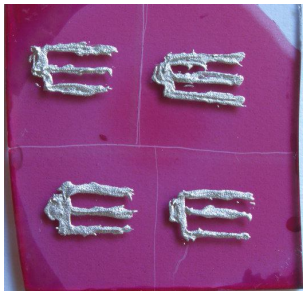

Figure 55: Painted solvent-free silver paste (E10-101) used as top electrode.

Figures 56(a) and (b) are the front and back view pictures and (c) is the optical image of thermally evaporated aluminum of ~100nm thick, used as the top electrode which showed good device characteristics and no penetration to the bottom contact.

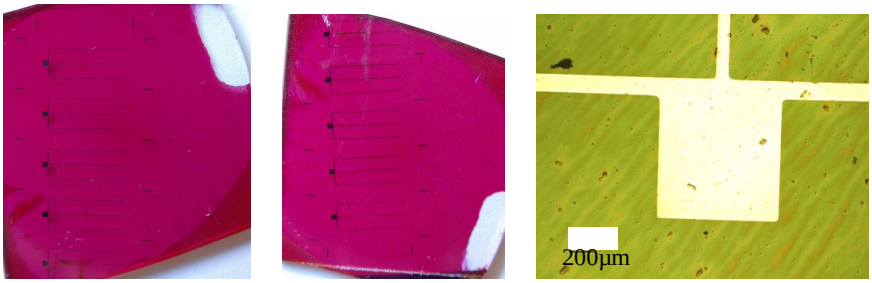

(a) (b) (c)

Figure 56: Evaporated aluminum (a) front view (b) back view (c) Optical image

4.9 Cell Measurements

Cells were fabricated using P3HT-PCBM in different compositions of 66-33 wt%, 50-50 wt% and 33-66 wt%. This absorber layer was deposited on ITO coated with PEDOT-PSS and DNA-CTMA hole transport layers. For each hole transport layer, five

samples were made that were annealed at 100 °C for different annealing times of 40minutes, 30minutes, 20minutes, 10minutes, and 5 minutes. So, for each composition of the absorber layer there were 10 samples fabricated. Cell characteristics of all 30 devices resulting from three different compositions of the absorber layer were measured using two point probe set up. For each blend composition of the P3HT-PCBM, the output characteristics of the best cells (with respect to open circuit voltage) respectively with DNA-CTMA and PEDOT-PSS hole transport layers is reported here.

The measurements are carried out for 3 different conditions namely,

Dark Current – In this, the measurement is carried out inside the dark box without illuminating light on the cell. The current generated is the dark current.

Photo current – Under this condition, photocurrent is measured while external bias is applied to the cell.

Light- Under this condition, photocurrent is measured without applying external bias. Resistance of the circuit is controlled to measure the 4^{th} quadrant of the I-V curve, which is a typical output characteristic of the solar cell. In convention, the 4^{th} quadrant is flipped into the 1^{st} quadrant.

When the cell measurements were carried out, working cells were not obtained but the rectifying behavior and some photovoltage (~ 200 mV) was observed for cells made with PEDOT-PSS and DNA-CTMA. Most of the time, the open circuit voltage was possibly coming from an unknown capacitance. All the devices become quite leaky under light, but this leaky current works as an output power. Further study is necessary to find out the origin of the voltage for measurement carried out under dark. The dark

current from DNA-CTMA devices is comparable to that of the PEDOT-PSS devices, but no conclusion can be drawn from these results.

The cells with P3HT-PCBM (66-33 wt %), both PEDOT-PSS and DNA-CTMA cases showed comparable results. It is observed that the devices from both hole transport layers are leaky. For PEDOT-PSS layer, V_{oc} was about 341mV and I_{sc} was about 19nA compared to the case with DNA-CTMA layer in which V_{oc} is 327mV and I_{sc} is 32nA (Figure 57). By comparing results from different blend ratios, it is observed that the short circuit current in the case of DNA-CTMA layer is higher than that observed for PEDOT-PSS based cells and open circuit voltage is higher in case of PEDOT-PSS than DNA-CTMA based cells. The reason for this is still unclear and further study has to be done. But, the results may give indirect evidence of hole transport in the DNA-CTMA layer.

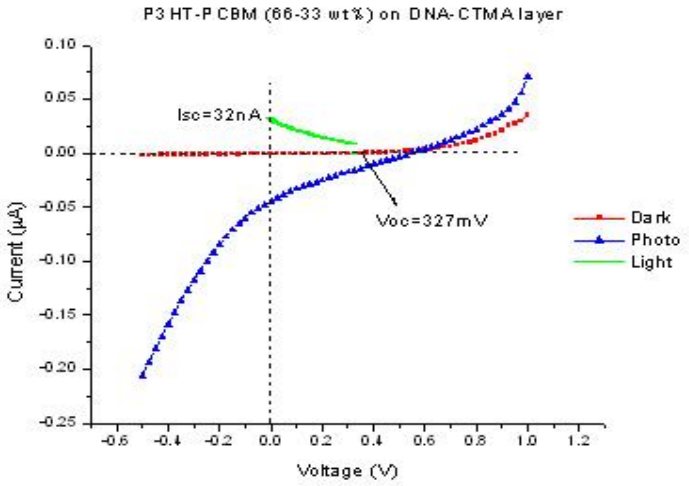

(a)

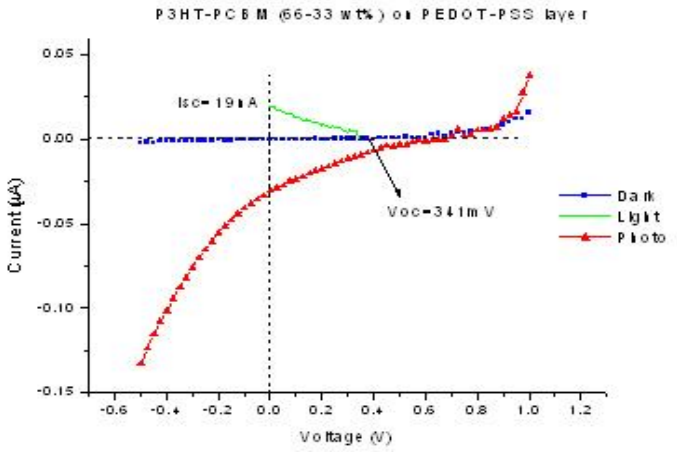

(b)

Figure 57: I-V characteristics of P3HT-PCBM (66-33 wt %) on (a) PEDOT-PSS and (b) DNA-CTMA hole transport layers.

For the cells with P3HT-PCBM (50-50 wt%) on PEDOT-PSS layer showed the highest V_{oc} of 215mV and I_{sc} of 11nA compared to the case with DNA-CTMA layer in which V_{oc} is 187mV and I_{sc} is 43nA (Figure 58).

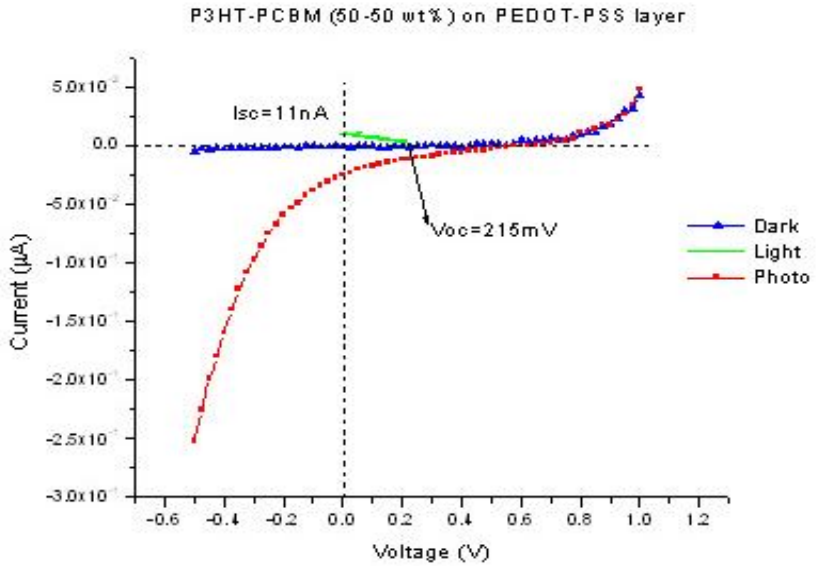

(a)

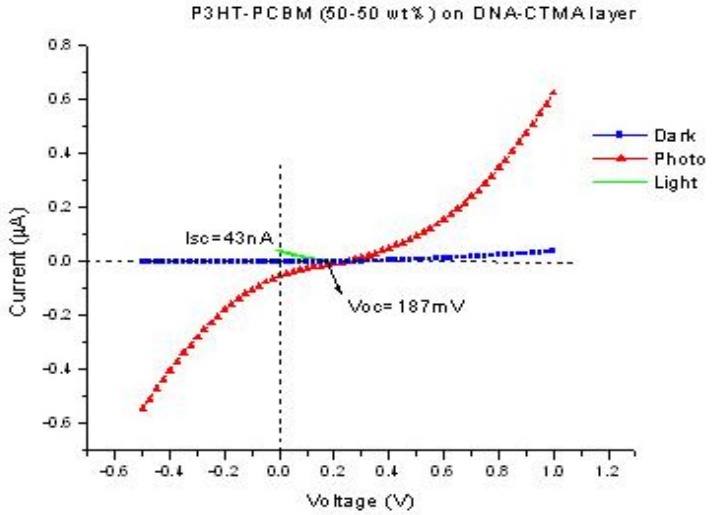

(b)

Figure 58: I-V characteristics of P3HT-PCBM (50-50 wt %) on (a) PEDOT-PSS and (b) DNA-CTMA hole transport layers

For the cells with P3HT-PCBM (33-66 wt%) on PEDOT-PSS layer showed the highest V_{oc} of 520mV and I_{sc} of 60nA compared to the case with DNA-CTMA layer in which V_{oc} is 227mV and I_{sc} is 380nA (Figure 59).

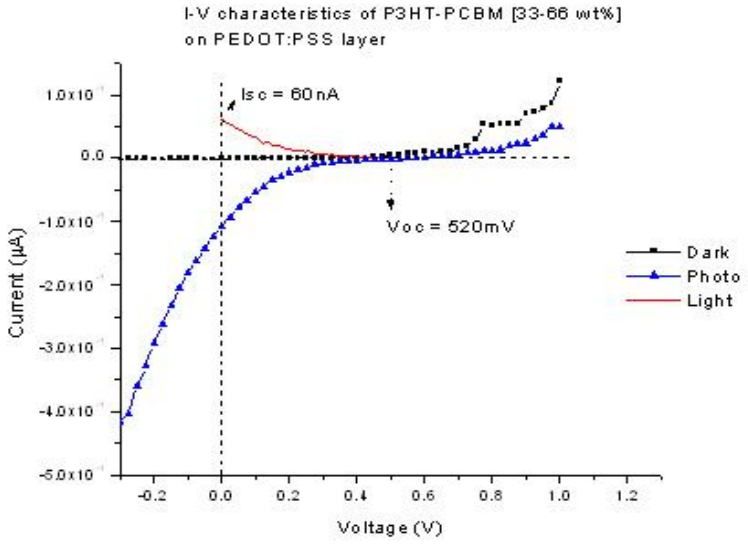

(a)

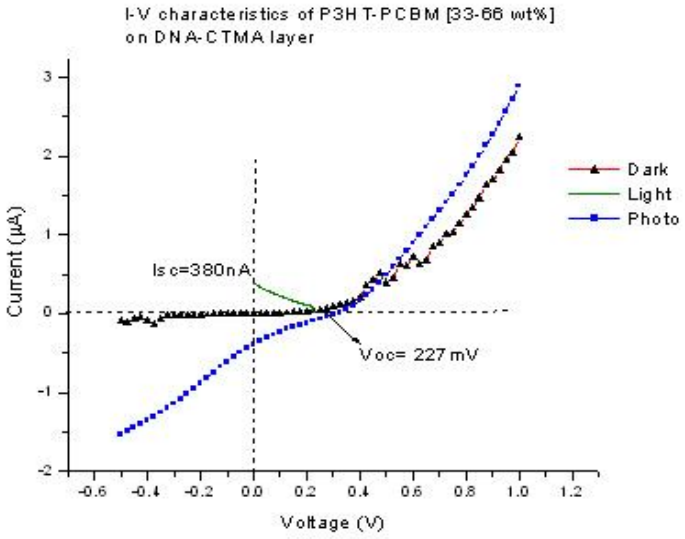

(b)

Figure 59: I-V characteristics of P3HT-PCBM (33-66 wt %) on (a) PEDOT-PSS and (b) DNA-CTMA hole transport layers.

CHAPTER 5

CONCLUSION

In the presented research, the thin-film of DNA-CTMA was used and investigated as a hole transport layer in bulk heterojunction polymer solar cells by replacing PEDOT-PSS, the commonly used hole transport layer in the field. Cyclic voltammetry carried out for DNA complex layer shows an oxidation peak which is seen from the oxidation of the guanine bases in DNA, in turn used to find the HOMO level of DNA complex layer and to construct the band alignment of the solar cell. From the optical transmittance of DNA complex layer, its band gap is extracted which is around 4.1 eV and this high band gap makes DNA transparent in the broad range of visible and in UV light.

FTIR results have confirmed the presence of the surfactant attached to the DNA molecules by providing the vibrational signal of the surfactant molecule. The ICPMS results show that the amount of sodium present is very low in DNA-CTMA complex when compared to DNA, indicating the replacement of sodium with the CTMA.

Optical images result show the formation of needles while using chloroform and chlorobenzene as the solvent, but is very high in case of chlorobenzene. In addition, the PCBM micro-needle formation was observed in the absorber matrix which increased with increasing annealing time and also the PCBM content in the P3HT-PCBM blend.

While using chloroform as the solvent, DNA-CTMA substrates showed less needle formation compared to PEDOT-PSS substrates. The optimum condition to prevent needle formation is not yet known and needs further study.

From the Photoluminescence measurements, we have observed quenching of the luminescence spectra in the P3HT-PCBM blend films when compared with that of pure P3HT films. This indicates that the excitons are dissociating to form free charge carriers.

From the I-V characteristics, the devices with DNA-CTMA and PEDOT-PSS showed nice rectifying behavior with reasonable photo voltage. The solar cells with a PEDOT-PSS layer showed V_{oc} up to around 500 mV and cells with DNA-CTMA layers up to about 327 mV. Further study needs to be done to understand the hole conduction in DNA-CTMA layer. Future research will further optimize the device performance.

REFERENCES

1. J. Nelson, The physics of solar cells, Imperial College Press, UK, (2003).
2. http://en.wikipedia.org/wiki/Solar_cell
3. S.O. Kasap, Optoelectronics and photonics: principles and practices, Upper Saddle River, NJ : Prentice Hall, (2001).
4. http://www.pmodwrc.ch/pmod.php?topic=tsi/composite/SolarConstant
5. http://www.csr.utexas.edu/projects/rs/hrs/process.html
6. http://www.nasolar.com/images/solargraph.gif
7. H. Hoppe and N. S. Sariciftci, Organic solar cells: An overview, *J. Mater. Res*., **19**, 1924 (2004).
8. M. Grätzel, MRS Bulletin, **30**, 23 (2005).
9. C. J Brabec and S.N. Sariciftci, Conjugated Polymer Based Plastic Solar Cells, in: Semiconducting Polymers, (Federal Republic of Germany) (2001).
10. Brabec, Plastic Solar Cells, *Adv. Funct. Mater.* **11,** 15 (2001)
11. J. H. Schon, Ch. Kloc, and B. Batlogg, Efficient photovoltaic energy conversion in pentacene-based heterojunctions, *Appl. Phys. Lett.* **77**, 2473 (2000).
12. K. Petritsch, Organic Solar Cell Architectures, PhD Thesis, Technisch-Naturwissenschaftliche Fakultät der Technischen Universität Graz (Austria) (2000).

13. S.A. Jenekhe and S. Yi, Efficient photovoltaic cells from semiconducting polymer heterojunctions, *Appl. Phys. Lett.* **77**, 2635 (2000).
14. D. Meissner and J. Rostalski, Highly efficient molecular organic solar cells, Proceedings of the 16th European photovoltaic solar energy conference, Glasgow (2000).
15. C.W. Tang, Two-layer organic solar cell, *Appl. Phys. Lett.* **48**, 183 (1986).
16. K, Petritsch, Dye based donor/acceptor solar cells, *Solar Energy Materials & Solar Cells* **61**, 63 (2000).
17. D. Wöhrle, Investigation of n/p-Junction Photovoltaic Cells of Perylenetetracarboxylic Acid Diimides and Phtalocyanines, *J. Mater. Chem.* **5**, 1819 (1995).
18. P. Peumans and R. Forrest, Very-high-efficiency photovoltaic cells, *Appl. Phys. Lett.* **79**, 126 (2001).
19. J.J.M, Halls, Efficient photodiodes from interpenetrating polymer networks, *Nature* **376**, 498 (1995).
20. G. Yu and J. Heeger, Charge separation and photovoltaic conversion in polymer composites with internal donor/acceptor heterojunctions, *J. Appl. Phys.* **78**, 4510 (1995).
21. G. Yu, Polymer Photovoltaic Cells: Enhanced Efficiencies via a Network of Internal Donor-Acceptor Heterojunctions, *Science* **270**, 1789 (1995).
22. M. Granström, Laminated fabrication of polymeric photovoltaic diodes, *Nature* **395**, 257 (1998).

23. S. E. Shaheen, 2.5% efficient organic plastic solar cells, *App. Phys. Lett.* **78**, 841 (2001).

24. I. Kanzan , R. Ulbricht, and A. Zakhidov, High efficiency P3HT/PCBM Solar Cell, *Mater. Res. Soc. Symp. Proc.* **836**, L3.2.1 (2005).

25. L. Gang, V. Shrotriya, J. Huang, Y. Yao, T. Moriarty, K. Emery and Y. Yang, High-efficiency solution processable polymer photovoltaic cells by self-organization of polymer blends, *Nature Materials*, **4**, 865 (2005).

26. J. Y. Kim, K. Lee, E. Nelson, Coates, D. Moses, T. Nguyen, M. Dante, A J. Heeger, Efficient Tandem Polymer Solar Cells Fabricated by All-Solution Processing, *Science* **317**, 222 (2007).

27. A. D. Bates and A. Maxwell, DNA topology, Oxford University Press, Oxford, (2005).

28. http://en.wikipedia.org/wiki/Nucleobase

29. http://www.oup.com/uk/booksites/content/0198506554/resources/storage/ma01f02.jpg]

30. R Gutiérrez1, D. Porath and G. Cuniberti, Introducing Molecular Electronics (Lecture Notes in Physics), Springer (2005).

31. R. G. Endres, D. L. Cox and R. R. P. Singh, Colloquium: The quest for high-conductance DNA, *Rev. Mod. Phys*. (**76**), 195 (2004).

32. J.M. Warman, M.P.de Haas, A. Rupprecht: DNA: a molecular wire, *Chem. Phys. Lett.* **249**, 319 (1996).

33. H. Wagenknecht, Charger transfer in DNA, Wiley-VCH, (2005).

34. http://physicsweb.org/articles/world/14/8/8

35. E. Braun, Y. Eichen, U. Sivan, and G. Ben-Yoseph, DNA-templated assembly and electrode attachment of a conducting silver wire, *Nature* **391**, 775 (1998).

36. D. Porath, A. Bezryadin, S. De Vries, and C. Decker, Direct measurement of electrical transport through DNA molecules, *Nature* **403**, 635 (2000).

37. Koyama, K. Hirata, T. Oyamada, T. Imai, H. Sasabe, and C. Adachia, Electroluminescence as a probe for elucidating electrical conductivity in a DNA-CTMA lipid complex layer, *Appl. Phys. Lett.* **85**, 9 (2004).

38. J.A Hagen, W. Li, A.J. Steckl and J.G. Grote, *Appl. Phys. Lett.* **88**, 171109 (2006).

39. A. Ashok, Thesis, Electrical Characterization of conjugated polymer light emitting devices (2004).

40. J.G. Grote, N. Ogata, J.A. Hagen, E. Heckman, P.P. Yaney, M.O. Stonne, Darnell E. Diggs, R.L. Nelson, J.S. Zetts, F.K. Hopkins and L.R.Dalton, *Molecular Crystals and Liquid Crystals* **426**, 3 (2005).

41. P. Stadler, Hysteresis in Bio-Organic Field-Effect Transistors, PhD Thesis, (2006).

42. E. M. Heckman, J. A. Hagen, P. P. Yaney, J. G. Grote and F. K. Hopkins, Processing techniques for deoxyribonucleic acid: Biopolymer for photonics applications, *App. Phys. Lett.* **87**, 211115 (2005).

43. L. Wang, J. Yoshida, N Ogata, S. Sasaki, and T. Kajiyama, *Chemistry of Materials* **13**, 1273 (2001).

44. A. F. Diaz, *Chem. Scr*. **7**, 142 (1981).

45. J. Roncali, *Chem. Rev*. **97**, 173 (1997).

46. T.A. Chen and R.Rieke, *J. Am. Chem. Soc*. **114**, 10087 (1992).

47. H. Sirringhaus, P.J. Brown, R.H. Friend, M.M. Nielsen, K. Bechgaard, B.M.W. Langeveld-Voss, A.J.H. Spiering, R.A.J. Janssen, E.W. Meijer, P. Herwig, and D.M. deLeeuw, *Nature* **401**, 685 (1999).

48. http://www.solennebv.com.

49. http://www.chm.bris.ac.uk/pt/diamond/mattthesis/chapter5_files/image001.gif

50. http://en.wikipedia.org/wiki/Cyclic_voltammetry

51. http://www.biol.paisley.ac.uk/marco/Enzyme_Electrode/Chapter1/Cyclic_Voltammetry1.htm

52. K. D. Dobson, A. D. Roddick-Lanzilotta, and A. J. McQuillan, An in situ infrared spectroscopic investigation of adsorption of sodium dodecylsulfate and of cetyltrimethylammonium bromide surfactants to TiO_2 , ZrO_2 , Al_2O_3 , and Ta_2O_5 particle films from aqueous solutions, *Vibr. Spec*. **24** 287 (2000).

53. M.R. Bugs and M.L. Cornelio, *Photochemistry and Photobiology* **74,** 512 (2001).

54. E. E. Ferapontova and E. Dominguez, *Electroanalysis* **15**, 7 (2003).

55. S.-W. Hwang and Y. Chen, Synthesis and Electrochemical and Optical Properties of Novel Poly(arylether)s with Isolated Carbazole and *p*-Quaterphenyl Chromophores, *Macromolecules* **34**, 2981 (2001).

BIOGRAPHICAL INFORMATION

Vidyalakshmi Kolachure was born in Mysore, India. She completed her Bachelor of Engineering in Polymer Science and Technology from Visveswaraiah Technological University, Belgaum, India. As part of her curriculum, she conducted projects in Central Food Technological Research Institute (CFTRI) and in J.S.S Pharmacy College, Mysore, on the use of polyvinylalcohol/chitosan blend films for drug delivery applications.

In fall 2005, she joined Material Science and Engineering as a graduate student to obtain Master's degree. She worked as a graduate research assistant in the Photovoltaics Materials Laboratory for two years. After completion of Master's degree, she is looking forward to work in a polymer or semiconductor industry.